AD-A115 193 BOSTON COLL CHESTNUT HILL MA SPACE DATA ANALYSIS LAB F/G 12/1
NUMERICAL AND DATA ANALYSIS TECHNIQUES APPLIED TO SCIENTIFIC RE--ETC(U)
AUG 81 N J GROSSBARD, M E STICK, B F SULLIVAN F19628-79-C-0063
UNCLASSIFIED BC-SDAL-81-5 AFGL-TR-81-0329 NL

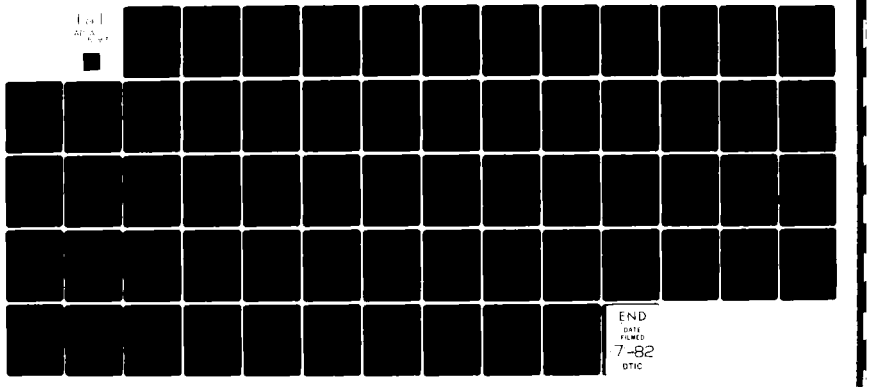

END
DATE FILMED
7-82
DTIC

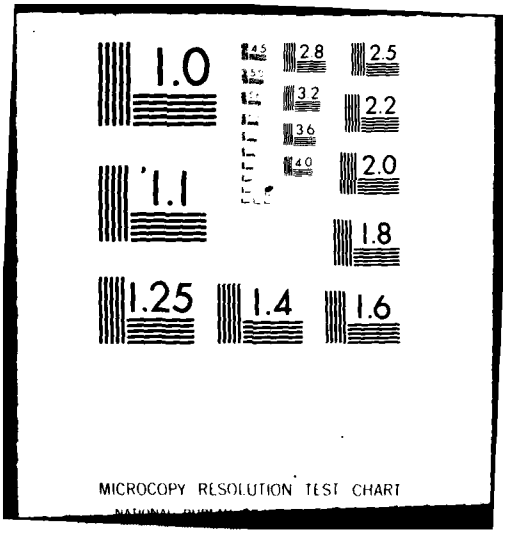
1.0
1.1
1.25
1.4
1.6
1.8
2.0
2.2
2.5
2.8
3.2
3.6
4.0
MICROCOPY RESOLUTION TEST CHART

AFGL-TR-81-0329

NUMERICAL AND DATA ANALYSIS TECHNIQUES APPLIED TO SCIENTIFIC RESEARCH - IV

Neil J. Grossbard
Marvin E. Stick
Brian F. Sullivan

Space Data Analysis Laboratory
Boston College
Chestnut Hill, Massachusetts 02167

Final Report
1 January 1979 - 31 March 1981

31 August 1981

Approved for public release, distribution unlimited

Air Force Geophysics Laboratory
Air Force Systems Command
United States Air Force
Hanscom AFB, Massachusetts 01731

UNCLASSIFIED

SECURITY CLASSIFICATION OF THIS PAGE *(When Data Entered)*

REPORT DOCUMENTATION PAGE	READ INSTRUCTIONS BEFORE COMPLETING FORM
1. REPORT NUMBER: AFGL-TR-81-0329	2. GOVT ACCESSION NO.: AD-A115 193
	3. RECIPIENT'S CATALOG NUMBER:
4. TITLE *(and Subtitle)*: NUMERICAL AND DATA ANALYSIS TECHNIQUES APPLIED TO SCIENTIFIC RESEARCH - IV	5. TYPE OF REPORT & PERIOD COVERED: Final Report 1 Jan '79 - 31 Mar '81
	6. PERFORMING ORG. REPORT NUMBER: BC-SDAL-81-5
7. AUTHOR(s): Neil J. Grossbard, Marvin E. Stick, Brian F. Sullivan	8. CONTRACT OR GRANT NUMBER(s): F19628-79-C-0063
9. PERFORMING ORGANIZATION NAME AND ADDRESS: Space Data Analysis Laboratory, Boston College, Chestnut Hill, MA 02167	10. PROGRAM ELEMENT, PROJECT, TASK AREA & WORK UNIT NUMBERS: 9993XXXX
11. CONTROLLING OFFICE NAME AND ADDRESS: Air Force Geophysics Laboratory, Hanscom AFB, Massachusetts, Contract Monitor: Mr. Edward Robinson (SUNY)	12. REPORT DATE: 31 August 1981
	13. NUMBER OF PAGES: 65
14. MONITORING AGENCY NAME & ADDRESS *(if different from Controlling Office)*	15. SECURITY CLASS. *(of this report)*: Unclassified
	15a. DECLASSIFICATION DOWNGRADING SCHEDULE

16. DISTRIBUTION STATEMENT *(of this Report)*

Approved for public release; distribution unlimited

17. DISTRIBUTION STATEMENT *(of the abstract entered in Block 20, if different from Report)*

18. SUPPLEMENTARY NOTES

19. KEY WORDS *(Continue on reverse side if necessary and identify by block number)*

Numerical Analysis	Data Analysis
Mathematical Analysis	Discrete Fourier Transform
Trajectory	Attitude Determination

20. ABSTRACT *(Continue on reverse side if necessary and identify by block number)*

This report describes the mathematical and numerical analysis techniques used in the solution of four of the major problem efforts engaged in under Air Force Contract F19628-79-C-0063. Although many other problems were solved under this contract, the analysis and techniques utilized were for the most part similar with variations to those described in the three previous reports (AFCRL-TR-73-0433, AFGL-TR-76-0091, and AFGL-TR-79-0132).

DD FORM 1 JAN 73 1473

UNCLASSIFIED

SECURITY CLASSIFICATION OF THIS PAGE *(When Data Entered)*

TABLE OF CONTENTS

TABLE OF CONTENTS (Cont.)

LIST OF FIGURES

LIST OF TABLES

ACKNOWLEDGEMENTS

The authors wish to express their thanks to Mr. Edward Robinson, Mr. Robert E. McInerney, and Dr. Randall Murphy of the Air Force Geophysics Laboratory (AFGL) for their assistance in the development of solutions to many of the problems considered under this contract. A similar debt of gratitude is owed to all Problem Initiators from AFGL for providing the detailed background information regarding their particular problems.

Mr. Leo F. Power, Jr., the Director of this laboratory, was invaluable in supplying the necessary resources to meet critical deadlines and finally, our appreciation goes out to the support staff of this laboratory for their continual assistance in the program preparation of these problems and in particular to Miss Mary Kelly for the excellent job of preparing this report for publication.

ATTITUDE DETERMINATION

Introduction

The orientation of the sensing axis of an instrument with respect to a fixed coordinate system in space is referred to as its attitude. From the attitude of a sensor, one may determine the angle it makes with any other vector such as the rocket's velocity vector, the sun line vector, etc. For certain sensors, meaningful interpretation of the instrument's output can be accomplished only when the attitude of the sensor axis is known.

Various types of gyroscopic platforms used as attitude measuring systems on vehicles are discussed. The systems include the Attitude Control System with two free gyros, the Miniature Attitude Reference System with segmented lengths over a 5 volt span for the roll, pitch and yaw axes, and the Miniature Inertial Digital Attitude System with a one-to-one correspondence between angular displacements and digital coding outputs.

The next discussion centers upon processing procedures which produce final attitude information from vehicle gyro measurements. An analysis is shown which relates any onboard probe vector $\hat{P}$ to the local coordinate system fixed at the launch site. With the orientation of $\hat{P}$ determined, the attack angle with any other attitude determined or predetermined vector can be supplied. Oftentimes, the initial orientations of onboard sensors require corroboration. A study is outlined to compare the phase relationship between onboard measurements and attitude predicted magnetic field, lunar, or solar intensities. This approach can be used for both side and axial output, but determination of phase angle variations are restricted to well-behaved areas of a vehicle's flight.

To provide continuous final output for the attitude system measurements, data refinement techniques are introduced with the calculation of statistical error values between the predicted and measured output. Tolerance levels are set on the measured input data to ensure that all predicted data will be within a specified σ deviation.

Gyroscopic Platforms Used as Attitude Measuring Systems

Attitude Control System

Space Vector Corporation's Attitude Control System (ACS) is comprised of a Roll Stabilized Platform (RSP) with two free gyros which output yaw, pitch and roll vehicle motion. Top dead center (TDC) of the gyro is the reference for all onboard probes (Figure 1). The roll and yaw are true measurements of vehicle motion but since there are only two free gyros, true vehicle pitch is a function of yaw. Further, if the vehicle yaws over 85°, this will cause loss of initial reference for the system and make attitude determination almost impossible.

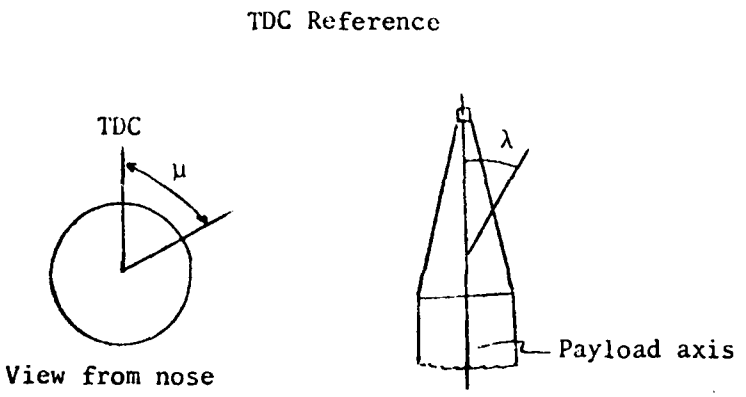

Top Dead Center Reference

Figure 1

Various models of the ACS were used as attitude measuring systems on the rockets analyzed. All ACS models function similarly but output differently. In some cases, the pitch and yaw coarse data were calibrated in .12 volt increments with a linear conversion range of ±90° corresponding to a 5 volt span. The pitch and yaw fine data over a similar volt span had a conversion range of ±5°. The roll telemetry data had a linear conversion range of ±180° on a 4.8 volt span.

According to Figure 2, pitch coarse for the ACS was decreasing voltage when pitching down, and a yaw right motion was increasing yaw coarse voltage. A clockwise roll viewed aft to nose was increasing voltage. Further, pitch fine was increasing voltage when pitching down, and a yaw right motion was decreasing yaw fine voltage.

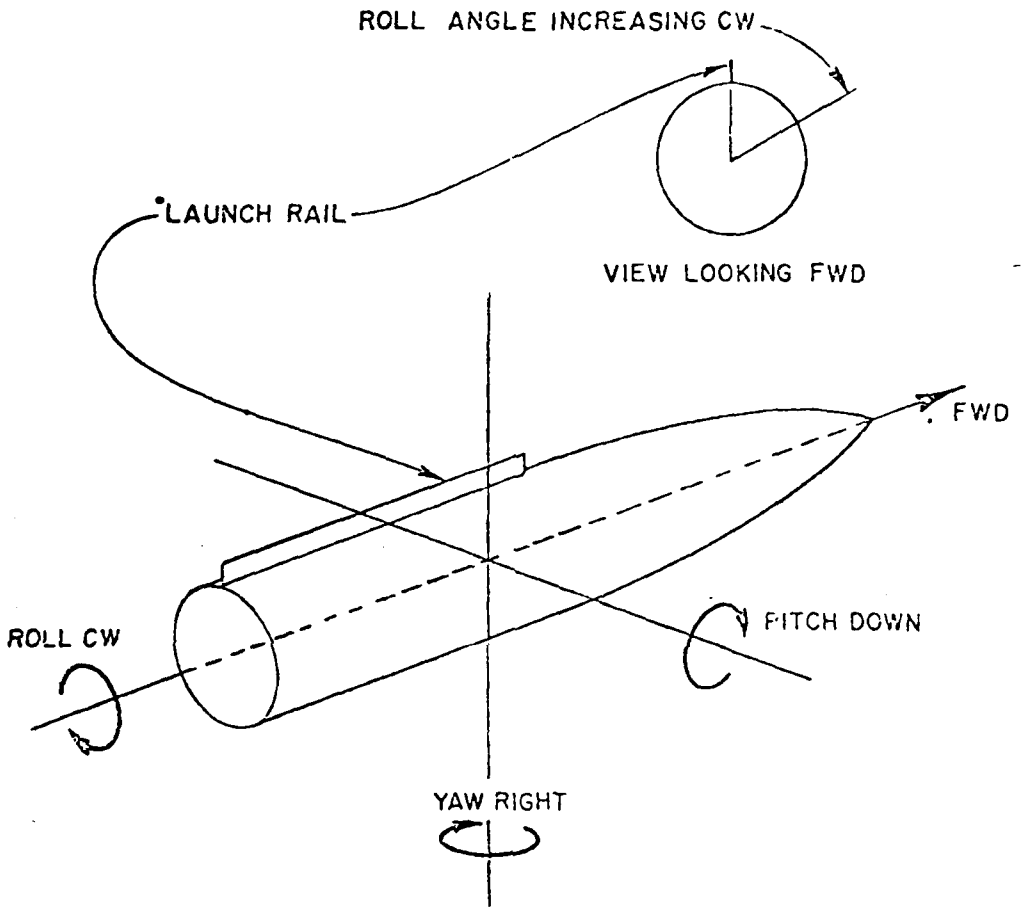

*LAUNCH RAIL = 0 degrees ROLL

ACS Coordinate Reference

Figure 2

In other cases, only pitch coarse, yaw coarse and roll gyro data were output. The pitch data was calibrated over a ±90° corresponding to a 5 volt span. However, to model the calibration information, discrete polynomial expressions were used over finite intervals. From 0 volts - 4 volts, a linear model was used and from 4 volts - 5 volts, a second degree model best represented the calibration information. The roll telemetry data had a linear conversion range of four 90° segments, each on a 5 volt span.

Other situations existed whereby gyro output consisted of pitch coarse, pitch fine, yaw coarse, yaw fine and roll gyro data. The pitch coarse segment was calibrated from -20° to +170° over a 5 volt span with decreasing voltage when pitching down. The yaw coarse segment was calibrated for a range of ±70° over a 3.3 volt span, i.e., .8 to 4.1 volts. A yaw right motion was decreasing voltage for the coarse yaw output. Selected data points were recorded for pitch fine data, and the model connecting each pair of points was essentially a straight line. However, no data calibration points were recorded for yaw fine. As previously described, pitch fine was increasing voltage when pitching down but yaw fine was now increasing voltage when yawing to the right. The roll segment was calibrated from 180° counterclockwise (CCW) to 178° clockwise (CW) over a 4.7 volt span with voltage decreasing for a CW roll when viewed aft to nose.

Another ACS gyro reference system consisted of pitch and yaw channel output at ±180° over a 5 volt span, and roll channel output at a 360° segment over a 5 volt span. Although not used in the data reduction, the pitch and yaw high resolution were ±10°. The zero reference for the gyro roll was the launch rail (Figure 3). Looking forward, yaw right is positive, pitch up is negative and roll clockwise is positive.

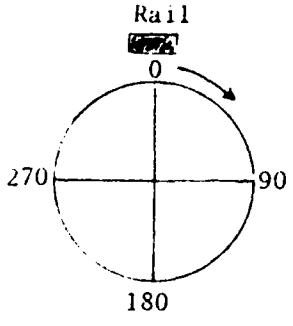

ACS Gyro Roll Zero Reference

Figure 3

MARS attitude system.

The Space Vector Corporation's Miniature Attitude Reference System (MARS) provided gyroscopic output for the determination of rocket attitude for various vehicles. The roll axis coincided with the rocket axis at launch and the orientation of a gyro reference notch was used to determine the location of the yaw axis. The cross product of the yaw axis with the roll axis yielded the pitch axis. The axes and rotations of the MARS system are identified in Figure 4.

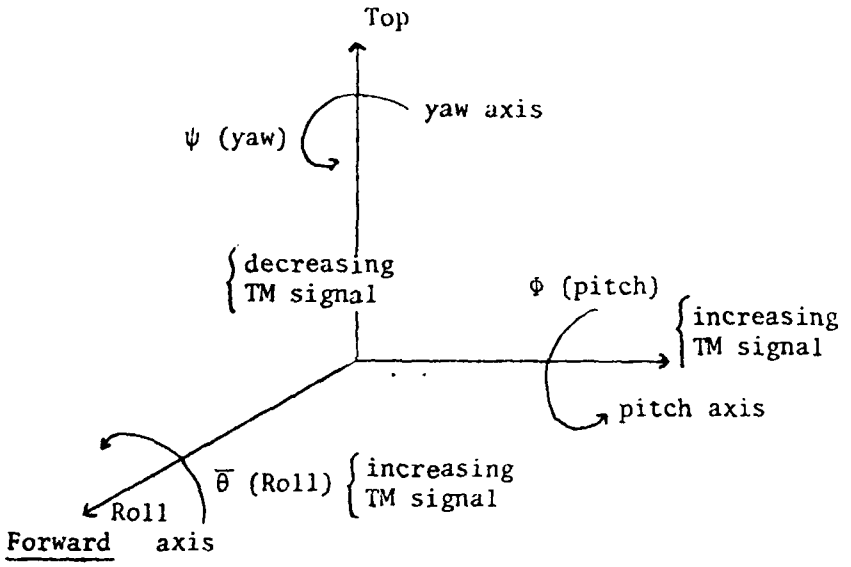

MARS Reference System

Figure 4

The segmented lengths over a 5 volt span for each MARS axis are:

a) Roll: 90°
b) Yaw: 60°
c) Pitch: 45° .

Segment identification of the pitch and yaw outputs for this system required continuous monitoring of the output to determine the precise time of transition from one segment to the next. By keeping track of the transitions and their

direction evidenced by a plus or minus 5 volt step change, one could correctly identify the segments presented. The roll output identification was a 5° ±3° shorted segment in the center of the 1st segment which appeared as a constant output voltage for that portion of the segment. This short was repeated every 4th segment.

MIDAS attitude system.

Space Vector Corporation's Miniature Inertial Digital Attitude System (MIDAS) provided gyroscopic output used to calculate the attitude of many rockets. The roll, pitch and yaw references were the same as for a MARS system but the outputs differed considerably. Whereas a MARS system output in a 5 volt span representing some degree segment having a predetermined length, the MIDAS system's roll, pitch and yaw measurements were digitized by optical encoders and resulted in a one-to-one correspondence between angular displacements and digital codings. For the digital coding variable n, the angular displacement ϕ in degrees was

$$\phi = \frac{n}{1024} \times 360 \quad .$$

No bias values were needed for conversion since the MIDAS system represents the displacement from the uncaged position of the gyro which fixes the coordinate reference system. The flow of attitude data for MIDAS vehicles is simplified considerably when compared with the flow of ACS and MARS vehicles.

Processing Procedures and Data Analysis

Processing procedures.

The oscillogram containing vehicle gyro measurements is inspected for inflight calibrations, data irregularities, gyro malfunctions, approximate spin rates, precessional period and half cone angle. The digital tape containing the gyro data is then unpacked and converted to degrees and plotted. These plots are then reviewed with results of the oscillogram inspection to identify obvious problems which will adversely affect the data processing.

If no gyro malfunction occurs then the quick-look attitude and angles of attack for the rocket axis are calculated based upon preliminary information. Should gyro malfunctions occur, procedures most appropriate to the available data are used to calculate the yaw, pitch, and roll information in the irregular area. If the attitude measuring system is a MIDAS, then attack angles for requested side probes are calculated at the same time as attack angles for the rocket axis. If attitude for side probes is requested for an ACS or MARS system, the roll data is converted to degrees, checked for proper conversion and then the preliminary side probe attitude is calculated.

All data irregularities and inflight calibrations are filtered from the gyro conversions and the results displayed. This output, if displaying a lack of continuity, is curve fitted by procedures most appropriate to the existing data pattern.

Finally, if onboard probes measure magnetic field, lunar, or solar intensities, it is possible to corroborate the calculated attitude. Depending upon the reliability of the onboard measurements, a standard error estimate of the attitude can be included as part of the normal output. A flow of the attitude data for both ACS and MARS vehicles is displayed in Figure 5, and a flow of the data for MIDAS vehicles in Figure 6.

Analysis.

Given the unit vectors $\hat{X}$, $\hat{Y}$, $\hat{Z}$ in the directions of the gyro roll, pitch (p) and yaw (y) axes, the direction of the longitudinal axis of the vehicle can be expressed as the vector e''_r:

$$e''_r = \hat{X} \cos y \cos p + \hat{Y} \sin y + \hat{Z} \cos y \sin p \qquad (1)$$

Flow of Attitude Data for ACS and MARS Vehicles

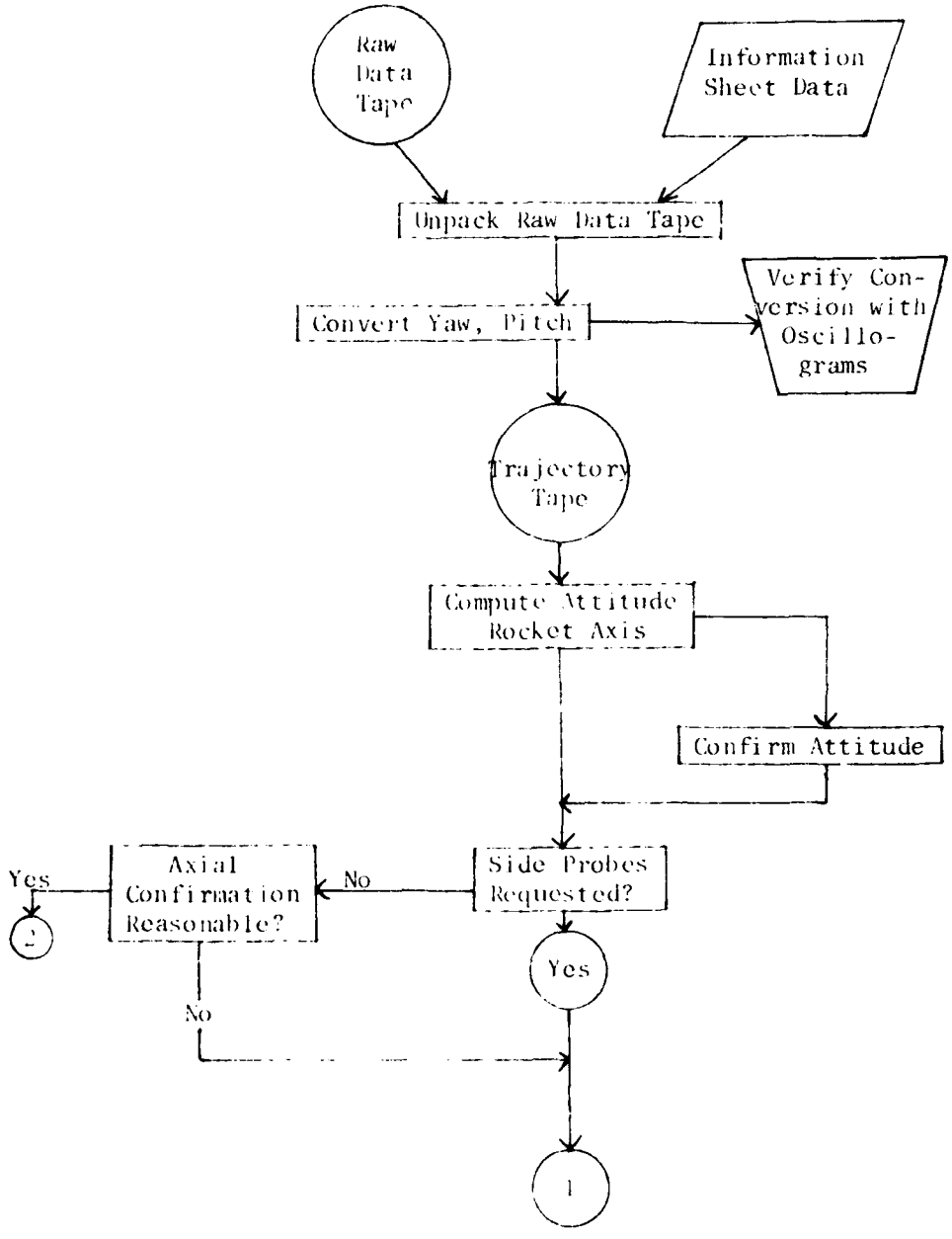

Flow of Attitude Data for ACS and MARS

Figure 5

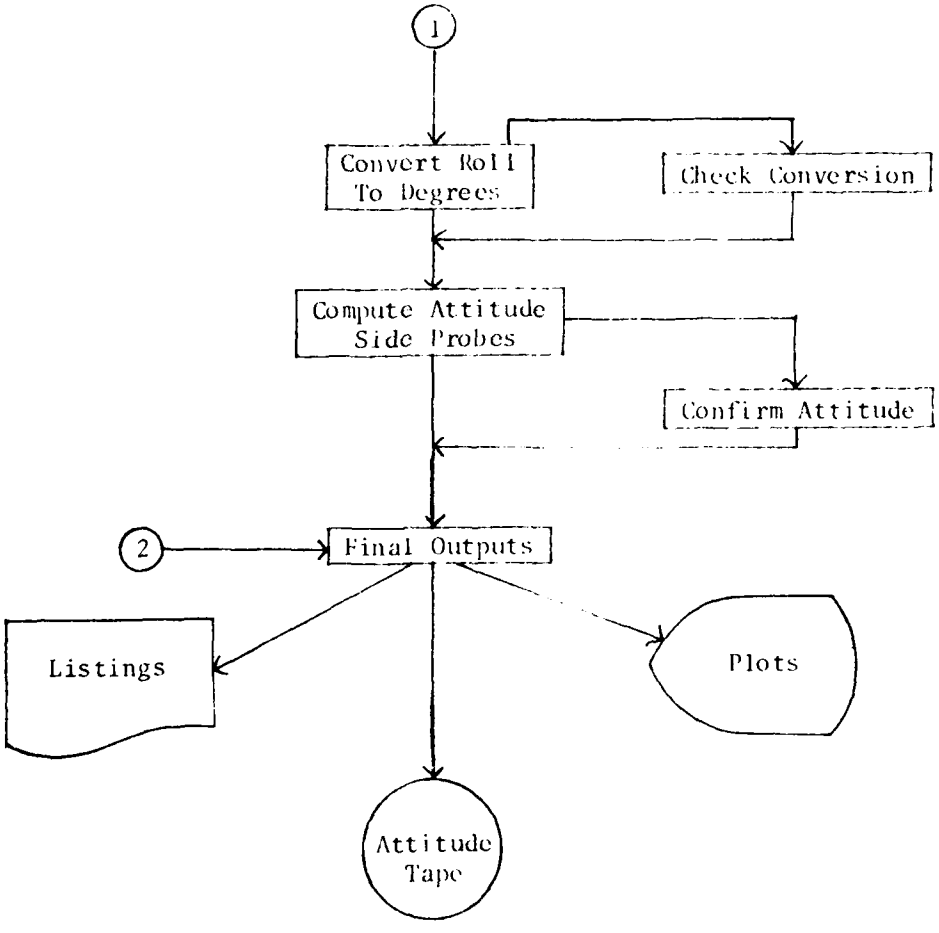

Figure 5 (Cont.)

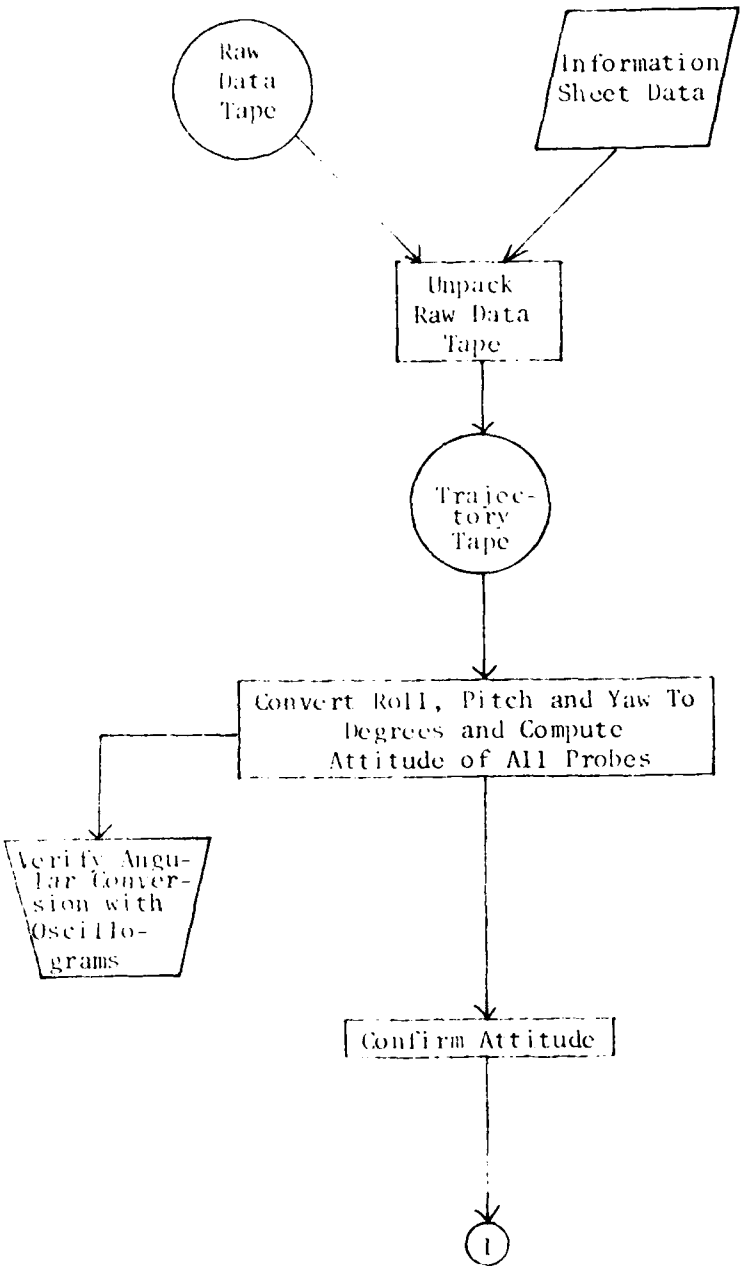

Flow of Attitude Data for MIDAS

Figure 6

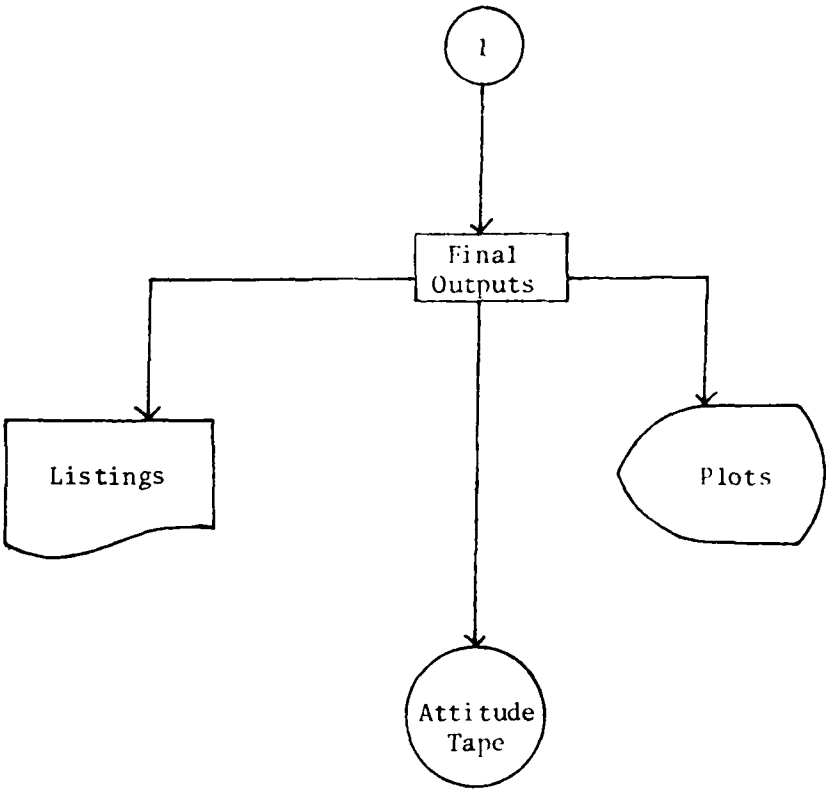

Figure 6 (Cont.)

where y and p are the true vehicle yaw and pitch respectively. Now let e_{ϑ_c}, e_{ϕ_c}, e_{r_c} be unit vectors in the directions of true North, East and the local vertical, fixed at the launch site. Within this system, the elevation of a vector is determined as the angle it makes with the local horizontal. The direction of the local vertical is positive elevation. The azimuth of a vector is the angle between its projection in the horizontal plane and e_{ϑ_c} measured positive clockwise from North (see Figure 7).

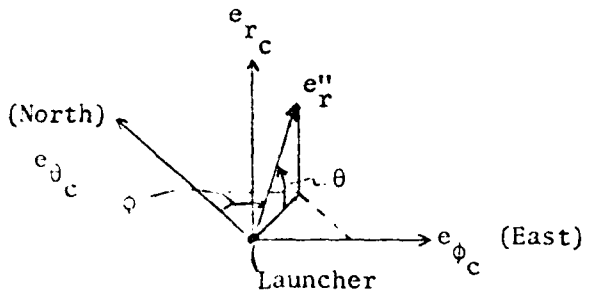

θ = Elevation of e''_r

ϕ = Azimuth of e''_r

Local East, North and Vertical System

Figure 7

Using the direction coefficients of the gyro axes at launch, the unit vectors $\hat{X},\hat{Y},\hat{Z}$ can be expressed as linear combinations of the earth-based system e_{ϑ_c}, e_{ϕ_c}, e_{r_c}. If we call the coefficient matrix B, then

$$\begin{bmatrix} \hat{X} \\ \hat{Y} \\ \hat{Z} \end{bmatrix} = B \begin{bmatrix} e_{\vartheta_c} \\ e_{\phi_c} \\ e_{r_c} \end{bmatrix}$$

We can define a system of orthonormal vectors e''_r, e''_1, e''_2 at any time in flight as a linear combination of the gyro axes. If A represents the coefficient matrix of the gyro output, then

$$\begin{bmatrix} e''_r \\ e''_1 \\ e''_2 \end{bmatrix} = A \begin{bmatrix} \hat{X} \\ \hat{Y} \\ \hat{Z} \end{bmatrix}$$

In particular, as described in (1)

$$a_{11} = \cos y \cos p$$

$$a_{12} = \sin y$$

$$a_{13} = \cos y \sin p \quad .$$

To transform the time dependent e''_r, e''_1, e''_2 system into the local e_{θ_c}, e_{ϕ_c}, e_{r_c} system, form the matrix product of A and B. Letting the matrix C = AB, then

$$c_{ij} = \sum_{m=1}^{3} a_{im} b_{mj} (i,j=1,2,3)$$

and

$$\begin{bmatrix} e''_r \\ e''_1 \\ e''_2 \end{bmatrix} = C \begin{bmatrix} e_{\theta_c} \\ e_{\phi_c} \\ e_{r_c} \end{bmatrix} \quad . \tag{2}$$

Once the attitude of the vehicle's main axis has been determined as direction cosines, the elevation and azimuth may be derived. From (2), we have

$$e''_r = e_{\theta_c} \cos\theta \cos\phi + e_{\phi_c} \cos\theta \sin\phi + e_{r_c} \sin\theta \quad .$$

Therefore:

$$\theta = \sin^{-1}(c_{13}) \quad ,$$

and

$$\phi = \tan^{-1}\left(\frac{c_{12}}{c_{11}}\right) \quad .$$

The elevation and azimuth of e''_1 and e''_2 are similarly derived.

In order to extend this approach to a vector $\hat{P}$ lying in the sensing direction of a probe having any orientation on the rocket, $\hat{P}$ is represented

$$\hat{P} = e''_r \cos\lambda + e''_1 \cos\mu \sin\lambda + e''_2 \sin\mu \sin\lambda \quad ,$$

where λ is the angle between e''_r and $\hat{P}$, and μ is the angle between e''_1 and the projection of $\hat{P}$ in the plane of e''_1 and e''_2. Furthermore, if θ_p and ϕ_p are the respective elevation and azimuth of $\hat{P}$, it follows that

$$\hat{P} = e_{\theta_c} \cos\theta_p \cos\phi_p + e_{\phi_c} \cos\theta_p \sin\phi_p + e_{r_c} \sin\theta_p \quad . \tag{3}$$

We can also define P_1, P_2, P_3 - the vector components of $\hat{P}$ - by the transformation:

$$\begin{bmatrix} P_1 \\ P_2 \\ P_3 \end{bmatrix} = \begin{bmatrix} d_{11} & d_{12} & d_{13} \\ d_{21} & d_{22} & d_{23} \\ d_{31} & d_{32} & d_{33} \end{bmatrix} \begin{bmatrix} e_{\theta_c} \\ e_{\phi_c} \\ e_{r_c} \end{bmatrix} \quad , \tag{4}$$

where each d_{ij} $(i,j=1,2,3)$ *is a product of* e_{ij} *and the corresponding direction* cosine of $\hat{P}$. Using the same technique as for e''_r, the coefficients of e_{θ_c}, e_{ϕ_c}, e_{r_c} in (3) and (4) are equated, readily yielding θ_p and ϕ_p

Finally, if V is any vector associated with the rocket flight, the angle between $\hat{P}$ and V may be derived. The unit vector in the direction of V is given by

$$\hat{V} = \frac{e_{\theta_c} v_1 + e_{\phi_c} v_2 + e_{r_c} v_3}{|V|} = e_{\theta_c} v'_1 + e_{\phi_c} v'_2 + e_{r_c} v'_3 \quad , \tag{5}$$

where the v_i $(i=1,2,3)$ terms are the components of $\hat{V}$ in the directions of north, east and vertical. The resulting v'_i terms are thus the direction cosines of $\hat{V}$.

The scalar product of (3) and (5) yields

$$\hat{P}\cdot\hat{V} = v'_1 \cos\theta_p \cos\phi_p + v'_2 \cos\theta_p \sin\phi_p + v'_3 \sin\theta_p \quad .$$

Hence, the angle ψ, between $\hat{P}$ and $\hat{V}$ is given by:

$$\psi = \cos^{-1}(v'_1 \cos\theta_p \cos\phi_p + v'_2 \cos\theta_p \sin\phi_p + v'_3 \sin\theta_p) \quad .$$

If the unit vector $\hat{V}$ is replaced by an offboard unit vector representing magnetic field, lunar, or solar intensities, then this offboard vector can take the form

$$\hat{H} = e_{\theta_c} h_1 + e_{\phi_c} h_2 + e_{r_c} h_3 \quad .$$

The geocentric coordinates together with the launch data determine the direction cosines h_1, h_2, h_3 of the offboard unit vector $\hat{H}$. The pitch angle between $\hat{H}$ and the onboard sensor $\hat{P}$ in the direction of the magnetometer, solar sensor, or lunar sensor is

$$\beta_1 = \cos^{-1}(\hat{H} \cdot \hat{P}) \quad .$$

However, the pitch angle β_2 can also be computed directly from onboard measurements as the $\cos^{-1}$ of the ratio of the intensity in the P direction to the total intensity. The pitch angles β_1 and β_2 are then compared to confirm the attitude data, and check for phase angle variations.

Data refinement.

Due to irregularities often present in the recorded data, filtering procedures are modified or developed as required to provide continuous final output for the attitude determination system. The primary routines used are Fourier Series, n^{th} degree polynomial approximations, and moving average methodology.

To provide smooth, continuous and acceptable attitude information for vehicles when they have established angular precessional velocity and a half cone angle, it is possible to generate gyro yaw and pitch information by means of the Fourier Series expansion. During this well-behaved area of a particular vehicular flight, the coarse and/or fine yaw and pitch data can be predicted by the Fourier Series

$$y = \frac{a_o}{2} + \sum_{n=1}^{\infty} \left(a_n \cos \frac{n\pi x}{L} + b_n \sin \frac{n\pi x}{L}\right) \quad .$$

This procedure has proven successful due to the periodic nature of the data. However, for most rocket flights, quick convergence of the Fourier Series is obtained with an approximation incorporating a linear term

$$y = f_1 + f_2 t + f_3 \sin\omega t + f_4 \cos\omega t \quad .$$

A preliminary angular velocity ω is selected from a study of the oscillograms of the raw data, and is further refined by an option within the fitting routine.

During regions in which a vehicle is not coning, yaw and pitch outputs are separated into discrete time intervals. These intervals are then curve fitted with polynomials up to the 9th degree when necessary. The n^{th} degree polynomial routine calculates an RMS value between measured and predicted data for each of the polynomial approximations. The minimum RMS value determines the degree of the polynomial approximation to be used in the specified interval.

Moving average methodology has also been used to correct for random noise. Variations have included n by m weighted procedures to follow true data patterns. This approach is used when continuous but irregular measurements are available, and smoothing is required.

Regardless of the refinement technique employed, a standard error estimate s is computed between measured and calculated values to compute an acceptable confidence interval. This confidence interval is used to select the optimum modeling approach among those under consideration.

Vehicles processed.

Using the procedures described in this report, 20 attitude reports for various vehicles have been prepared during the reporting period from 1 January, 1979 to 31 March, 1981. A listing of completed vehicle attitude appears in Table 1. Final outputs consists of launcher and vehicle referenced plots and listings of selected parameters. A final attitude tape containing all available time referenced outputs is also generated.

TRAJECTORY

Introduction

Raw radar or telemetry tracker recorded polar coordinate data for a rocket is normally available on magnetic tape. However, such tapes are not initially compatible with the Control Data Corporation (CDC) 60 bit word format. To enable processing of the data, the tape must be unpacked and rewritten in a CDC compatible form. Once unpacked, the data is examined for excessive noise and prolonged missing data intervals. If either condition exists, appropriate data plugging procedures are initiated prior to a geocentric coordinate conversion of the radar or tracker referenced slant range, azimuth, and elevation data.

In the event multi radar and/or tracker information is available, conversions of the available data to any desired reference location is possible. This transformation enhances the reliability of the filtering procedures when excessive noise or missing data in selected intervals cannot be modeled. In such cases, reliable positional data from appropriate radars and trackers are merged to form a continuous data base.

When an adequate model for the vehicle is available, normal data filtering procedures consist of optimizing the launch conditions to the start of the filter limits by back filtering the data to launch. When a model is not available, then a double filter is normally performed. This procedure back filters the positional data to only the start of the filter limits. In both cases, either integration or data reproducing options are available beyond the filter limits.

Final outputs for the rocket trajectory system consist of filtered positional values referenced to the launcher and the radar. Residual data during the back filter period is also available.

Radar and Tracker Systems

Several tracking systems have been employed during this reporting period. A brief description of the primary unpacking routines for these systems follows:

1. RTMIN - used for real time radar data from White Sands. Positional values are launcher referenced.

2. REFORMS - used to reformat radar referenced data received from the Wallops Flight Center (WFC).

3. REFORMN - used to reformat DNA tracker data from Poker Flat Research Range.
4. REFORMO - used to unpack telemetry tracker data from the Oklahoma State University (OSU) Tradat system.
5. 3x80 - used to reformat single radar tracking data from White Sands.
6. 3x80 MULTI - used to reformat multi radar tracking data from White Sands.

Additional features were incorporated into the 3x80 multi unpacking routine in order to more adequately compare the vehicle trajectory results from each radar employed. Residuals between x,y,z and $\dot{x},\dot{y},\dot{z}$ are calculated and plotted for desired pairs of radars. These displays are used as aids in judging which radar is most reliable.

The unpacked data is written in 16x6 blocks with radar referenced time, slant range, azimuth, and elevation data being the normal configuration in each 16 word record. In the event excessive noise or missing data exists for any of the parameters in this file, data plugging and modeling procedures are used to rewrite the 16x6 data file in a form compatible with the remainder of the trajectory processing system.

Processing Procedures

Should excessive missing data or noise exist in the unpacked data, dependence on a single modeling procedure for the ill behaved areas are often insufficient to produce reliable results. Hence, prior to geocentric conversion of the vehicle positional data, care is taken to provide a most complete and reliable estimate of the slant range, azimuth, and elevation information over time.

Data modification.

To correct extremely random data patterns requires either establishing a confidence band for acceptable values or generating a time series model through the data. In the case of establishing a confidence band, a weighted moving average of the data in selected intervals is created. The residuals between the raw and moving average data are then calculated and a standard error estimate σ is computed. A 95% confidence interval for acceptable measurements is normally established. Any time related raw positional value outside this interval is deleted from data base of acceptable values, and is replaced by the weighted moving average value.

When existing data patterns are readily obvious, but still randomness exists over extended periods, polynomial regression procedures are an alternate data modification method to the establishment of confidence bands for acceptance or rejection of the data. In such cases, higher ordered polynomials are successively passed through the data being examined. Residual error between the raw and calculated data is determined by the RMS value. The minimum RMS is the criterion for selection of the appropriate polynomial model.

To fill missing data intervals (greater than 10 seconds), polynomial modeling is used only when data patterns are quite apparent. In the event of irregular motion when multi radar information is available, reliable positional data from appropriate radars and trackers are merged to form a continuous data base prior to the data modification methodology. This procedure requires a coordinate transformation of the radar or tracker information to the desired reference point.

Transformation of positional information.

Given two or more sets of positional information for a given vehicle from different reference points, merging of selected intervals from each data base may be accomplished in order to generate a more continuous and reliable file of positional information. Assuming the geodetic latitude, longitude, and height above the Earth's surface of the given reference point to be

θ_1 : latitude

ϕ_1 : longitude

H_1 : height,

and the reference of the desired system to be θ_2, ϕ_2, and H_2, the goal is to transform the given slant range, azimuth, and elevation data to the new location. The raw positional data shall be designated as

SR_1 : slant range

A_1 : azimuth

E_1 : elevation ,

and the desired information as SR_2, A_2, E_2.

In the geocentric system, the vector to the target vehicle is defined as

$$R = r(i\cos\theta_L\cos\phi_L + j\cos\theta_L\sin\phi_L + k\sin\theta_L) \tag{6}$$

where

$$r = \sqrt{x^2 + y^2 + (z+r_o)^2}$$

$$x = SR_1 \cos E_1 \sin A_1$$

$$y = SR_1 \cos E_1 \cos A_1$$

$$z = SR_1 \sin E_1$$

$$r_o = 6378.185 - 21.39 \sin^2\theta_g .$$

The angles θ_L and ϕ_L are the geocentric latitude and longitude of the target vehicle. The geodetic latitude θ_g is computed as

$$\tan\theta_g = 1.006674 \tan\theta_L .$$

Furthermore, given the geocentric latitude θ_1 and longitude ϕ_1 of the initial radar/tracker,

$$\sin\theta_L = \frac{y\cos\theta_1 + (z+r_o)\sin\theta_1}{r}$$

$$\tan\phi_L = \frac{-y\sin\theta_1\sin\phi_1 + x\cos\phi_1 + (z+r_o)\cos\theta_1\sin\phi_1}{-y\sin\theta_1\cos\phi_1 - x\sin\phi_1 + (z+r_o)\cos\theta_1\cos\phi_1} \tag{7}$$

From (6), the components of the geocentric referenced position update vector are

$$XV = r\cos\theta_L\cos\phi_L$$

$$YV = r\cos\theta_L\sin\phi_L$$

$$ZV = r\sin\theta_L .$$

The problem is now to find a transformation matrix K to transform the original radar/tracker site data to the desired site. To calculate SR_2, A_2, and E_2 for the offset site where

$$AE2 = SR_2 \cos E_2 \sin A_2$$

$$AN2 = SR_2 \cos E_2 \cos A_2 \qquad (9)$$

$$AV2 = SR_2 \sin E_2 \quad ,$$

we must first express the local system components AE2, AN2, AV2 at the offset site in terms of available information. In matrix form, let

$$\begin{pmatrix} AE2 \\ AN2 \\ AV2 \end{pmatrix} = K \left[\begin{pmatrix} XV \\ YV \\ ZV \end{pmatrix} - \begin{pmatrix} X_{os} \\ Y_{os} \\ Z_{os} \end{pmatrix} \right] .$$

Computation for the Euler matrix K and offset vector X_{os}, Y_{os}, Z_{os} follow.

In the i,j,k geocentric system, let P_1 be the position of the initial radar/tracker and P_2 the position of the desired offset site.

$$P_1 = (R_1+H_1)\ (i\cos\theta_1 \cos\phi_1 + j\cos\theta_1 \sin\phi_1 + k\sin\theta_1)$$

$$P_2 = (R_2+H_2)\ (i\cos\theta_2 \cos\phi_2 + j\cos\theta_2 \sin\phi_2 + k\sin\theta_2) \quad .$$

The radii R_i are computed as

$$R_i = 6378.185 - 21.39 \sin^2\theta_{g_i} \quad , \quad i=1,2$$

where θ_{g_i} is the geodetic latitude of the respective radar/tracker.

The offsets from the geocentric to the offset location on the Earth's surface are

$$X_{os} = (R_2+H_2) \cos\theta_2 \cos\phi_D$$

$$Y_{os} = (R_2+H_2) \cos\theta_2 \sin\phi_D$$

$$Z_{os} = (R_2+H_2) \sin\theta_2$$

where ϕ_D is the longitude offset from the initial radar/tracker to the offset site.

The distance vector D (Figure 8) between P_1 and P_2 is defined as

$$D = P_2 - P_1$$

$$D = i[(R_2+H_2)\cos\theta_2\cos\phi_2 - (R_1+H_1)\cos\theta_1\cos\phi_1]$$
$$+ j[(R_2+H_2)\cos\theta_2\sin\phi_2 - (R_1+H_1)\cos\theta_1\sin\phi_1] \quad (10)$$
$$+ k[(R_2+H_2)\sin\theta_2 - (R_1+H_1)\sin\theta_1] \quad .$$

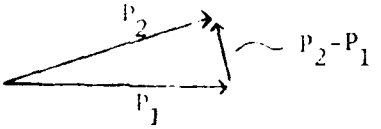

Vector Difference Between Radars

Figure 8

Simplifying equation (10) in terms of direction cosines,

$$\hat{D} = \frac{I}{|P_2-P_1|}\ (a_1 i + a_2 j + a_3 k)$$

where

$$|P_2-P_1| = \sqrt{a_1^2 + a_2^2 + a_3^2} \quad .$$

In the i,j,k system, the distance vector can also be expressed

$$\hat{D} = i\cos\theta_D\cos\phi_D + j\cos\theta_D\sin\phi_D + k\sin\theta_D \quad .$$

Equating the two expressions for $\hat{D}$,

$$\theta_D = \sin^{-1}\left(\frac{a_3}{|P_2-P_1|}\right)$$

$$\phi_D = \tan^{-1}\left(\frac{a_2}{a_1}\right) \quad .$$

These rotation angles θ_D and ϕ_D relate the local components at the desired offset site to the original site information as

$$\begin{pmatrix} AE2 \\ AN2 \\ AV2 \end{pmatrix} = \begin{pmatrix} -\sin\phi_D & \cos\phi_D & 0 \\ -\sin\theta_D \cos\phi_D & -\sin\theta_D \sin\phi_D & \cos\theta_D \\ \cos\theta_D \cos\phi_D & \cos\theta_D \sin\phi_D & \sin\theta_D \end{pmatrix} \begin{bmatrix} XV - X_{os} \\ YV - Y_{os} \\ ZV - Z_{os} \end{bmatrix} \quad (11)$$

Equating systems (9) and (11), the desired parameters at the new site are

$$SR_2 = \sqrt{AE2^2 + AN2^2 + AV2^2}$$

$$A_2 = \tan^{-1} (AE2/AN2)$$

$$E_2 = \sin^{-1} (AV2/SR2).$$

Corrections for extended missing data intervals, extreme data irregularity, and merging of multi radar information having been made, the trajectory data flow now continues with the geocentric conversion of positional values (see Figure 9).

Using corrected radar or tracker slant range, azimuth and elevation data the next phase of trajectory determination calculates geocentric position and velocity information as well as geodetic altitude of the vehicle. Using a four point cubic polynomial, further adjustments to the raw positional data can be made if necessary. Listings and displays are reviewed for data stability and completeness before continuing with the filtering procedures to produce final trajectory data.

Filtering.

Depending whether or not a model for vehicle dynamics exists, the corrected data base consisting of time, slant range, azimuth, and elevation data is passed through an appropriate filtering procedure. When a model does exist, a launch optimizing procedure is normally performed. In this case, filter limits are set, and the launch conditions are optimized to the start of the filter. When a model is not available, a double filter which back filters the positional data to only the start of the filter limits is the normal procedure. Filter limits are normally selected as the interval of well-behaved performance, and in all cases include data above 50 kms.

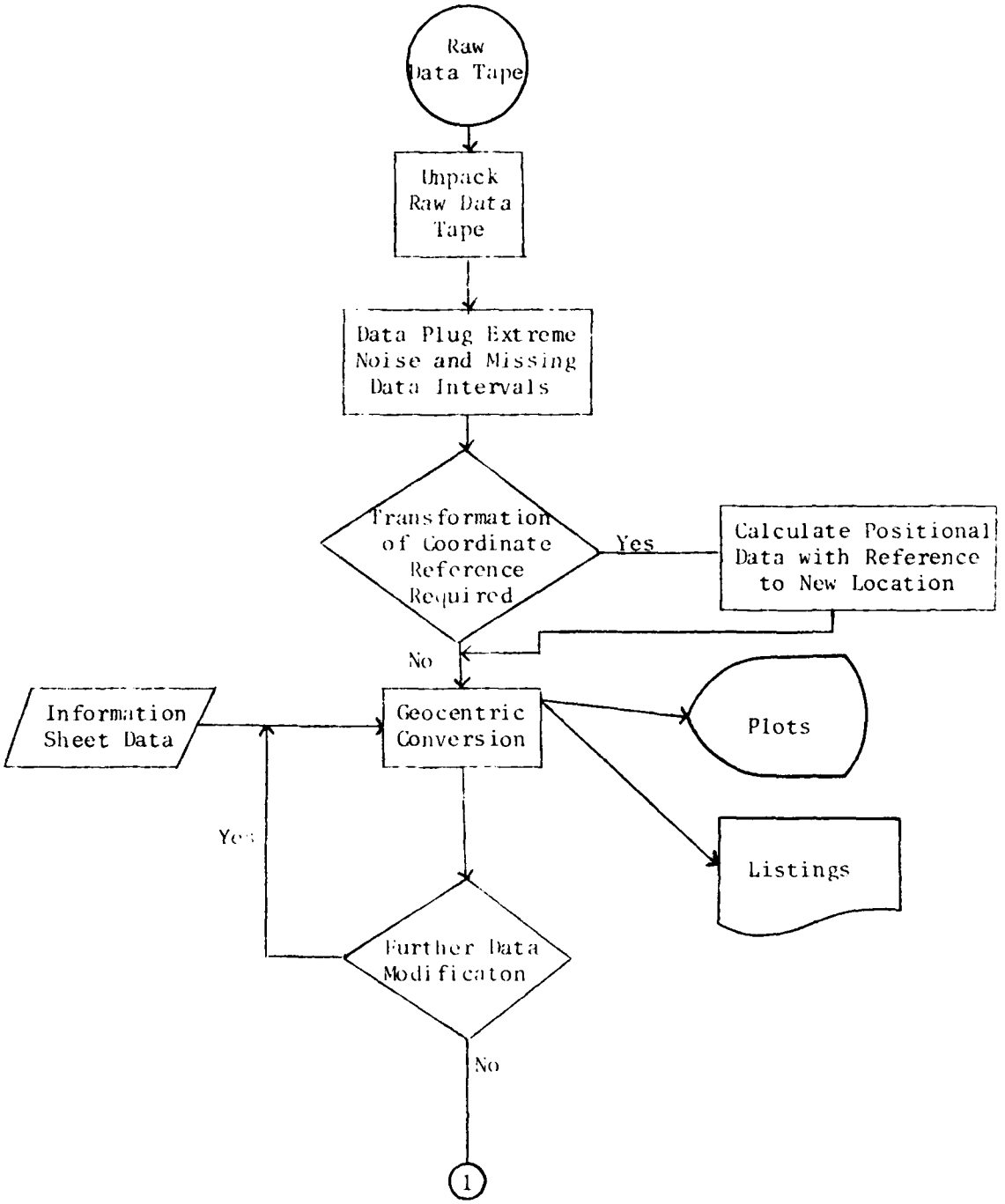

Flow of Trajectory Data

Figure 9

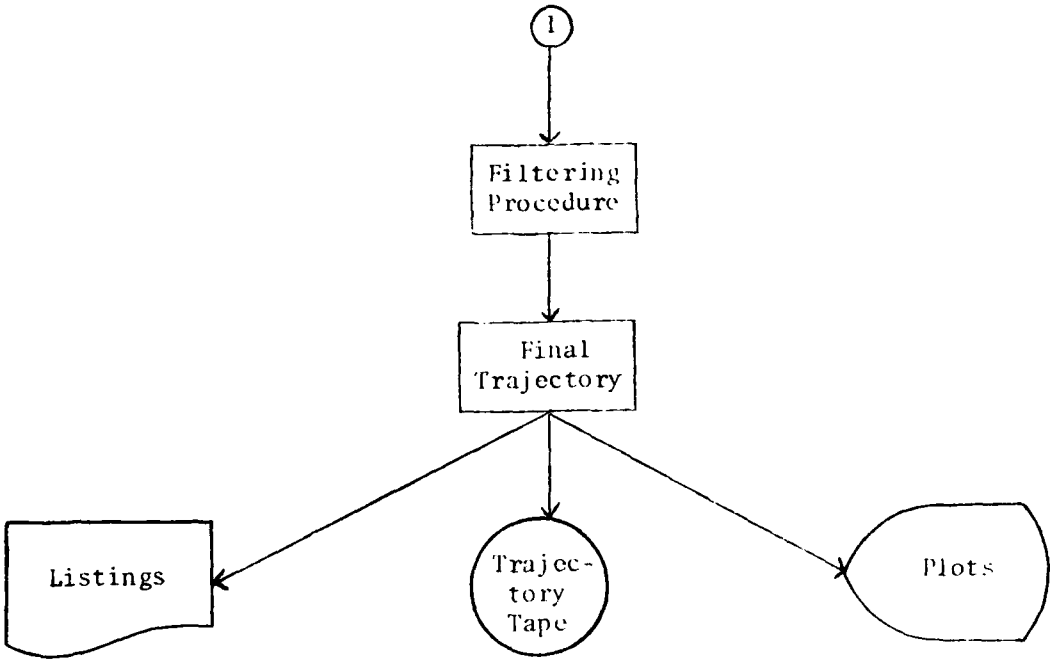

Figure 9 (Cont.)

Regardless of the filtering procedure, both integration and data reproducing options are considered to optimally complete the vehicle trajectory at low altitudes (below 40 kms). Often, increasing adjustments to the base angular variance are necessary for relatively smooth launcher referenced velocities. Examination of the plotted results and analysis of the data structure normally suggest the required adjustments at this phase.

Vehicles processed.

Using the procedures described in this section of the report, 18 trajectory reports have been prepared during the reporting period from 1 January, 1979 to 31 March, 1981. A listing of completed trajectories appear in Table 1. Final outputs consist of launcher and radar referenced plots and listings of selected positional parameters. A final trajectory tape containing all available time referenced filtered outputs is also generated.

Table 1

COMPLETED ATTITUDE AND TRAJECTORY REPORTS

Vehicle	Attitude	Trajectory
A24.609-2 (MSMP)		
Booster	x	x
Target	x	x
Sensor	x	x
IC819.08-1		
Nose cone	x	x
Payload	x	x
IC807.15-1	x	x
IR807.57-1	x	x
A10.802-1	x	x
A10.802-2	x	x
A07.712-1		x
A08.705-2		x
A08.708-1		x
A12.9A1		x
A12.9A2	x	x
A24.7S2-1		x
A18.805		
MIM	x	
PIM	x	x
A31.702	x	x
A04.703	x	
PLUMEX1	x	
PLUMEX2	x	
WS834.28-2	x	
WS834.28-3	x	
A10.901-1	x	x
A51.970 (EXCEDE II)	x	*

*Due to special data problems encountered, efforts are continuing in the determination of reliable positional information for EXCEDE II.

ANALYSIS TECHNIQUES APPLIED TO BALLOON-BORNE MOSAIC INTERFEROMETER AND RADIOMETER MEASUREMENTS

Computational techniques developed for the reduction and analysis of interferometer and radiometer data from the Balloon Altitude Mosaic Measurements (BAMM) program are presented. Emphasis is given to the reduction and analysis techniques developed for mosaic detector interferometer measurements. The presentation includes discussion of techniques to quality check, edit and simulate radiance values. Statistical analyses performed on simulated radiance data is described and examples of raw and edited data and statistical parameters are given. A brief discussion of radiometer reduction and analysis techniques is presented which includes data editing; filtering and decimation; statistical parameter determination; autocovariance estimation; and Fourier Power Spectral estimation of radiance.

Introduction

This discussion concerns the digital signal processing techniques developed to analyze and reduce radiometer and interferometer measurements into radiance. The use of interferometer measurements allowed the determination of the radiance values over any wavelength band(s). These radiance profiles are then statistically analyzed. The initial major concerns in developing the analysis were the magnitude of the error that would be added to the data base, because of the mathematical limitations of the techniques utilized and computer time. These concerns were minimized by the fact that the noise inherent to the experiments dominated those that would be introduced by the mathematical models. The procedures and computer coding were developed to minimize the amount of computer time and place some limitation on the computer storage used.

Since the analysis required the calculation of many discrete Fourier Transforms, it was essential to develop a fast version of the Fast Fourier Transform. (The Fast Fourier Transform is an algorithm for rapidly calculating Discrete Fourier Transforms.) The routine developed minimizes the time spent deciding which "butterfly" (butterfly refers to a logical procedure used many times in the Fast Fourier Transform technique) to calculate next. Other

techniques such as suggested by Morris[1], are available but the one used was judged the fastest given the computer storage limitations.

Data characteristics.

The sample rate for the radiometer data base (one sample every .0073 seconds) was such that very little aliasing (ambiguity in deciding at which frequencies the Fourier Power exists) occurred. Further, there was negligible Fourier Power near the Nyquist Frequency (the highest frequency inherent in the Discrete Fourier Transforms).

The interferometer measurements consisted of a "scan" every Δt seconds. Sixteen simultaneous interferograms were generated for each scan (only the central 4 detectors were used in a rapid scan mode). Each detector, however, is processed individually. The focal plane consisted of a 4×4 mosaic array of detectors, hence for the two scan rates Δt, was either .25 seconds or .0575 seconds. A scan consisted of measurements of the interferograms starting at maximum optical retardation and moving to the other extremum. The next scan repeated the process heading in the opposite direction. Limitations in the equipment meant that the time interval between every other scan was constant. The time interval between consecutive scans, however, was a function of the direction. Similarly, the mechanical position corresponding to the zero optical retardation for every other scan was reproducible but differed for the two scan directions.

The sample rate for measurements for each scan was high enough to prevent aliasing. Δt was short enough that changes in the interferometer pattern during a scan could be ignored and further, that only a small amount of aliasing occurred when analyzing a set of scans. When events occurred, however, Δt was not short enough to assume that there was negligible Fourier Power near the Nyquist Frequency of a set of interferometer scans.

Filtering and decimation.

The processing of the edited radiometer data takes large amounts of computer time. In order to speed the processing, the highest frequency of interest was determined. Given this highest frequency (F_p) a low-pass filter

was designed and applied to the data. The filter used was designed to fit the following frequency response curve in a least square sense.

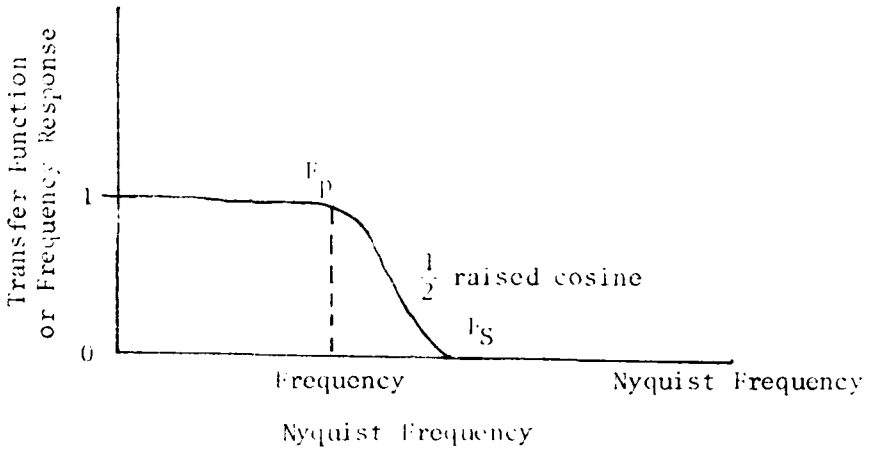

Figure 10

Here F_S was arbitrarily chosen approximately equal to 1.1 F_p. This filter was a symmetric finite impulse response filter. Enough coefficients were used so that the response curve nearly coincided with the above model.

This filter was applied in frequency space using the convolution theorem. The filtered data base was then decimated (every Nth point used) so that the new Nyquist frequency of the new data base was F_S, the start of the stop band of the discrete filter (Fourier Power above F_S approximately 0.). This procedure prevents any significant aliasing of the decimated data base. The amount of decimation was generally not a whole number of data points. In order to find the value between filtered data points, as specified by the decimation, linear interpolation was used. The radiometer values after filtering did not have a large amount of Fourier Power at frequencies near F_S. This meant that linear interpolation added negligible error to the analysis.

Data Processing Approach

The original radiometer data base occurred at approximately equally spaced time intervals. Thus we had data pairs R_i, t_i where R_i is the radiance reading at time t_i. In the original data base some of the R_i values were unavailable and others appeared to be unrealistic. Three reasons for unrealistic ("bad") measurements are possible. One is that the data is "stationary" and the

measurement is real. The odds of this happening are negligible (less than one in ten thousand) with this analysis. A second explanation is that the "bad" points are "gliches" in the measurements due to problems in the collection, transmission, digital conversion or processing of the data. The procedure attempts to remove these "gliches". The third explanation is that the "bad" points are actual "events". In order to see if "events" are removed by the editing procedure the effect of editing on measurements of known "events" was checked. The method selected for editing the data involved first differences and as proceeded follows:

1) Calculate

$$A = \frac{1}{N_s} \Sigma((R_j - R_1)/(j-i)$$

where the sum is for all pairs of points satisfying the following criteria. R_j and R_i are available, $j>i$ and $j-i$ the minimum such value. N_s is the number of terms in the sum.

2) Similarly calculate

$$MS = \frac{1}{N_s} (((R_j - R_i)/(j-i))^2)$$

3) Remove "bad" R_i values until all the remaining points satisfy the criteria

$$|((R_j - R_i)/(j-i)) - A| \leq \sqrt{MS} * S$$

where S is a parameter set to 4.

For the radiometer this editing had no discernible effect on known "events".

After "bad" points were removed from the radiometer data base the missing radiance values are filled in using linear interpolation. As long as there are no long time intervals where the data was missing and there is negligible Fourier Power near the Nyquist frequency linear interpolation was sufficient.

Radiometer or Radiance Calculated from Interferometer Intensity

Statistical estimates were used as tools to validate or formulate theories of how the actual data behaved. The estimates used in our processing are exceedance (EX), Probability, Autocovariance (AU), and a Power Spectral Density (PSD).

Estimating exceedance.

Exceedance is defined as EX(X) = 1-F(X) with F(X) the cumulative probability function.

The following method of estimating the exceedance of (RAD) (radiance values) was used:

1) Estimate the mean as $AVE = \frac{1}{N} \sum Y_i$

where Y_i are the RAD values and N is the number of measurements

2) Estimate the standard deviation as

$$\sigma = \sqrt{\sum (Y_i - AVE)^2/(N-1)}$$

3) Divide the interval $-3\sigma + AVE$ and $3\sigma + AVE$ into 400 equally wide bins. Add one additional bin for all values less than $-3\sigma + AVE$. Order these bins according to their radiance values. Place and count the Y_i values into their appropriate bin (BIN_j) where j=1,2,...,401)

4) The exceedance at the high edge of the j^{th} bin $E(RAD_j)$ is then estimated as

$$EX(RAD_j) = 1 - \frac{\sum_{\ell=1}^{j} BIN_\ell}{N}$$

Estimating probability.

The probability of radiance occurring in a particular interval was estimated using the first three steps in the exceedance estimation, with a smaller number of bins. These values could also have been calculated from estimates of the probability density function, which could be estimated by several different methods

Estimating autocovariance.

The autocovariance function of a set of discrete data (Y_i) is

$$AU(\tau) = E((Y_i - \bar{Y})(Y_{i+\tau} - \bar{Y}))$$

where $\bar{Y}$ is the mean of Y_i and E is the expected value and τ is known as the lag.

Two methods of estimating the autocovariance of the radiance were used. The estimates are:

Estimate (1)

$$AU^{(1)}(\tau) = \frac{1}{N} \sum_j ((Y_j - AVE)\ (Y_{j+\tau} - AVE))$$

which is a biased estimate of the autocovariance and estimate (2)

$$AU^{(2)}(\tau) = \frac{1}{N - |\tau|} \sum_j ((Y_j - AVE)\ (Y_{j+\tau} - AVE))$$

which is an unbiased estimate of the autocovariance. It should be noted that AVE could be replaced by some higher order curve fit of the data and that other reasonable estimates of AU are possible.

Estimating Power Spectral Density

The integral of the Power Spectral Density between some frequencies f_1 and f_2 is the energy found in that frequency interval. The total energy is assumed to equal $E((Y_i - \bar{Y})^2)$. Where E is the expected value and $\bar{Y} = E(Y_i)$.

Three methods of estimating the Power Spectral Density of RAD values were used. In all these methods the final results were normalized.

Let $P_i^{(s)}$ be the unnormalized Power Spectral Density estimates of RAD where $P_i^{(s)}$ is the s^{th} type estimate of the Fourier Power in the frequency (f) interval; $(i-1)*\Delta f \leq f - \frac{\Delta f}{2} < i*\Delta f$. Here Δf is the resolution frequency of the Fourier Power estimates. Then multiply $P_i^{(s)}$ by a constant $N^{(s)}$ such that

$$N^{(s)}\ \Delta f \sum_{i=1}^{L} P_i^{(s)} = \frac{1}{N} \sum_{j=1}^{N} (Y_j - AVE)^2$$

where $L*\Delta f$ is the Nyquist Frequency. The estimates $P_i^{*(s)} = N^{(s)}\ P_i^{(s)}$ are the normalized Fourier Power Estimates.

This normalization was used rather than attempting to estimate the weighting factor of any apodization (windowing) or smoothing performed to find the Fourier Power Estimates.

The three methods used to estimate the unnormalized Fourier Power were:

Method I - Raw Periodogram Estimates

The periodogram estimate involves finding discrete Fourier Coefficients of RAD and using the square of these coefficients as the unnormalized Fourier Power estimate.

Method II - Estimate from Bias Autocovariance

This method involved truncating $AU^{(1)}(\tau)$ to form $B(\tau)$, $B(\tau)$ is then apodized using a triangular window (Bartlett Window), although other apodizations could have been used. The unnormalized Fourier Power estimates were the cosine series coefficients of the resultant values.

Method III - Estimate from Unbiased Autocovariance

This method is exactly the same as Method II but applied to $AU^{(2)}(\tau)$.

In general the three methods usually lead to approximately equal values.

It should be noted that, there are other methods of estimating the Fourier Power by fitting the data to models. Some of the more popular such methods are known as Maximum Entropy, Maximum Likelihood and the Autoregressive Moving Average methods of Fourier Power Estimation.

The estimates calculated by these three methods might be improved by pre-whitening (filtering the data to better approximate white noise) the data and then post-darkening (correcting the Power Spectral Estimates for the transfer function of the pre-whitening filter) the results.

Editing Interferometer Data

From each scan of interferometer data one value of simulated radiance for a particular frequency band(s) was determined. The sample rate of the scans is such that it was advisable to remove as few scans as feasible.

An interferogram often took the form that the ends of the data occurred at approximate nulls. In between the nulls, the data tended to oscillate with larger and larger amplitude toward the center of the interferogram. When the data had nulls at its ends, a special editing technique was used to detect any unrealistic ("bad") points in the region of the nulls. This technique accepted measurements which either fell within a band around the value of the

approximate null or had a neighboring point with approximately the same value. Whenever a "bad" point was detected it was set to a neighboring value.

The measurements excluding any nulls was then arbitrarily divided into five equal segments. Each of these segments was edited separately. The editing of one of these segments involved finding the data point in this segment which caused the largest magnitude of first difference of the data. This point was deemed "bad" if the magnitude of the first differences associated with it was more than twice the magnitude of the neighboring first differences. Whenever a point was "bad", it was replaced using linear interpolation. After replacing a "bad" point, this algorithm was repeated for the same data segment. When the point checked was not "bad", the procedure was begun on the next data segment (if any). If there were an unacceptable number of "bad" points for the entire interferogram, it was ignored. For most cases the interpolation used added only a minute and tolerable changes to the low frequency behavior of the interferogram. In the case that one of the extremums (minimum of maximum) of the interferogram is found to be a "bad" point, this procedure would lead to an unacceptable measurement and rejection of this data. However, for all the cases checked, the extremums of the interferogram were not affected. After the initial editing was performed, the program logic searched for the center of the interferogram. The center is taken as the maximum excursion of the interferogram. The data was then truncated so that there were N points on either side of the center. Thus we have $2N+1$ points in a final edited interferogram. If the data did not have N points on either side of the center of the interferogram it was eliminated. This algorithm meant that we could compare many interferometer scans and be assured that the same type of data base was being analyzed. The resolution frequency of the data is improved to the degree the truncated interferograms occur at approximate nulls. To the degree data ends at nulls, leakage (Fourier Power from one frequency appears at neighboring frequencies) is minimized.

Interferometer Fourier Analysis

It is necessary to estimate values of the amplitude and phase of the Discrete Fourier Transform in order to calculate radiance values from the interferometer measurements.

Estimating amplitude.

The resolution frequency of the results of a Fast Fourier Transform equals $\frac{1}{\Delta X * J}$ where J is the number of points used in the Fast Fourier Transform. In this particular Fast Fourier Transform the number of points used was $J=2*4^T$ (T any integer). To decrease the resolution frequency of the Fourier Transform (not the data) and to use the Fast Fourier Transform subroutine as efficiently as possible, the edited interferogram measurements were continued (padded) with zeros to form 2048 data values. The actual input data was supplied to the Fast Fourier Transform (FFT) as follows.

Let RE be the real part of the input data of the FFT and TIM the imaginary part of the input data which is assumed complex (Otnes and Enochson[2]). Y_i is the padded data base with the center at Y_M. We then put

Y_M into RE_1	Y_{M-1} into TIM_{1024}
Y_{M+1} into TIM_1	Y_{M-2} into RE_{1024}
Y_{M+2} into RE_2	Y_{M-3} into TIM_{1023}
Y_{M+3} into TIM_2	Y_{M-4} into RE_{1023}
⋮	⋮
0 into TIM_{512}	0 into RE_{513} .

The results of the FFT, after unscrambling, give the amplitude and phase around the mid point of the interferogram.

Estimating phase.

From the results of the FFT, we get estimates of the phases of an interferogram. If the Y_M was found exactly at the center of the interferogram the phase estimates should be either 0 or ±180 degrees. The Y_i measurements, however, are taken at a spacing of ΔX and the value Y_M occurred somewhere in the interval $-\frac{\Delta X}{2} < X < \frac{\Delta X}{2}$ where X is the offset from the exact center of the interferogram. Thus a good approximation (under the assumption that the truncations occurred at equal distance from the center of the interferogram), the phase will be either $\frac{-X*\omega*180}{\Delta X*\omega_N}$ + noise or $-\frac{X*\omega*180}{\Delta X*\omega_N} \pm 180$ + noise, where ω is the frequency of the measurement and ω_N is the Nyquist frequency. The analysis only had to estimate where changes in the above phases occurred. Since the

resolution frequency of the interferogram was quite good, the phase changes usually occurred between consecutive estimates of the FFT. Occasionally, the changes occurred over two consecutive estimates of the phase.

Background Correction (instrument function)

The amplitude or intensity estimates ($A(\omega)$) of an actual experiment were corrected for the intensity inherent in the instrument. This made use of the knowledge of the phase estimates ($P(\omega)$) from the actual experiment. The procedure used was as follows:

1) Find $B(\omega)$ which are estimates of the amplitude of an experiment when the onboard interferometer looked at a cold source.
2) The values of $P(\omega)$ are estimated as either 0 + correction degrees (call 0) or ± 180 + correction degrees (call ± 180). Phase $P(\omega) = 0$ degrees was assumed for frequencies of between 0 and f_1. $P(\omega)$ was then assumed to be ± 180 from f_1 to some frequency f_2. It was then assumed to be 0 for all frequencies above f_2. The values of f_1 and f_2 were found by searching for values of the phase where $|P(\omega+2\Delta\omega)-P(\omega)| \geq 50$ degrees, where $\Delta\omega$ is the resolution frequency of the FFT. When $P(\omega)$ did not follow the expected pattern the scan was ignored.
3) Form corrected estimates $C(\omega)$ of $A(\omega)$ either $C(\omega) = |A(\omega) - B(\omega)|$ when $P(\omega) = 0$ or $C(\omega) = |A(\omega) + B(\omega)|$ when $P(\omega) = \pm 180$.

Estimating simulated radiance.

From values $C(\omega)$ (corrected intensity values) we can simulate radiance values. If we wish to simulate the discrete values of a radiometer which passes the frequencies between ω_L and ω_H we integrate values of $C(\omega)$ between ω_H and ω_L. This integral

$$\int_{\omega_L}^{\omega_H} C(\omega)\, d\omega$$

was numerically integrated using Simpson's Rule and/or a trapazoidal rule.

Editing simulated radiance values.

The editing of the simulated radiance used a similar procedure as the one used to edit the radiometer data with two changes. The first change was that the procedure was repeated whenever a "bad" point was detected until no additional "bad" points were detected. The second change was that whenever an

"event" seemed to occur after the initial editing, the simulated radiance values were processed without editing. This procedure was necessary because editing data from known events, although it left the event identifiable, removed some of the simulated radiance values during the event.

Conclusion

Interferometer experiments indicated that these results reproduce the measurements which would be obtained by a radiometer with any particular passband. This interferometer technique has the enormous advantage that any band may be selected via computer processing to provide information equivalent to several hundred individual radiometer measurements. The timing and positioning of the experiment described, however, was different according to which direction the interferogram was sampled. This led to Fourier Power near the Nyquist Frequency of the computed radiance. If this Fourier Power was ignored the resulting radiance values led to results which were consistent with the results of radiometer experiments. Other problems with this technique are that the analysis is not straightforward and a very large data base is needed for the computations.

Epilogue

Further relevant discussion and data analyses procedures will be presented in an AFGL technical memorandum dealing with a BAMM 3 data report.

References

1. Morris, L. R., "Automatic Generation of Time Efficient Digital Signal Processing Software", IEE Transactions on Acoustics, Speech and Signal Processing, Vol. ASSP-25, No. 1, February 1977.

2. Otnes, R. K. and L. Enochson, " Digital Time Series Analysis", John Wiley and Sons, 1972.

PRIMARY AURORAL ELECTRON PRECIPITATION PROBLEM AND ELECTRON AND PARTICLE DISTRIBUTION FUNCTIONS

Over the last two years mathematical and numerical analysis techniques have been applied to describe the effects of electrons in the ionosphere. In particular, two types of problems were studied. The electron and particle distribution functions in the ionosphere were predicted using computer code described in the Report AFGL-TR-79-0132. During the last two years this code was modified to incorporate the latest models for the collision and energy transfer cross sections for the particles in the ionosphere. In particular, referencing the report AFGL-TR-79-0132, $QI_{j,\ell}(E_i)$ is now calculated using either of two formulas. The first formula states that

$$\text{if } EI_{j,L} \geq E_i \text{ or } WI_{j,L} \geq E_i, \text{ then } QI_{j,\ell}(E_i) = 0 \quad .$$

Otherwise

$$QI_{j,L}(E_i) = Q0*FI_{j,L}/(I_{j,L}**2)*FX*\left(1 - \left(\frac{WI_{j,L}}{E_i}\right)^{AI_{j,L}}\right)^{BI_{j,L}}$$

where

$$FX = \left(\frac{WI_{j,L}}{E_i}\right) OI_{j,L} \text{ if } OI_{j,L} > .7 \ .$$

and

$$FX = \left(\frac{WI_{j,L}}{E_i}\right) * LN\left(4 *\left(\frac{OI_{j,L}*E_i}{WI_{j,L}}\right) + 2.718281828\right)$$

$$\text{if } OI_{j,L} \leq .7$$

Alternately the second formula states that $QI_{j,L}(E_i) = 0$ if $EI_{j,L} \geq E_i$.

$$\text{Otherwise } QI_{j,L}(E_i) = 10^{-16}*(KI_{j,L}/E_i)*LN\left(\frac{E_i}{JI_{j,L}}\right)*(GSI_{j,L}*E_i/(E_i+GBI_{j,L}))*$$

$$(\tan^{-1}((.5*(E_i-EI_{j,L})-(TSI_{j,L}-(TAI_{j,L}/(E_i+TBI_{j,L}))))/$$

$$((GSI_{j,L}*E_i)/(E_i+GBI_{j,L})))+\tan^{-1}(TSI_{j,L}-(TAI_{j,L}/(E_i+TBI_{j,L})))$$

$$*(E_i+GBI_{j,L})/(GSI_{j,L}*E_i))$$

In these representations $EI_{j,L}$, $GSI_{j,L}$, QO, $GBI_{j,L}$, $TBI_{j,L}$, $TSI_{j,L}$, $KI_{j,L}$, $JI_{j,L}$, TAI_{ij}, $WI_{i,j}$, $EI_{i,j}$, $OI_{i,j}$, $AI_{i,j}$, and $BI_{j,L}$ are input data values.

Another modification was a redefinition of $Q_{T,K}$, in particular for T=1, 2 or 3. The new formula takes the form

$$Q_{T,K} = 0 \text{ if } E_i \leq E_{T,K} .$$

$$\text{Otherwise } Q_{T,K} = QO*A_{T,K}/(II_{J,K}^2)*FX*\left(1-\left(\frac{II_{T,K}}{E_i}\right)^{B_{T,K}}\right)^{N_{T,K}}$$

where

$$FX = \left(\frac{II_{T,K}}{E_i}\right)^{O_{T,K}} \quad \text{if } O_{T,K} > .7$$

and

$$FX = \left(\frac{II_{T,K}}{E_i}\right) * LN\left(4. * \frac{O_{T,K}*E_i}{II_{T,K}} + 2.718281828\right)$$

$$\text{if } O_{T,K} \leq .7$$

In addition some values of $Q_{T,K}$ which were originally found by formulas are now supplied as tables of values versus E_i. These and other changes were made to the computer model. Drum plots were also made for all the cross-sections now used by this model.

The second major effort performed for this problem was calculating electron and/or proton fluxes in auroral electron/proton precipitation. Several mathematical models describing this problem have been studied. The following discussion describes the model upon which greatest efforts were expended to determine the electron flux.

Let this electron flux be $\phi(\tau,E,\mu)$ where τ is optical depth; E is the energy; and μ is the cosine of the zenith angle. Then a transport equation describing the electrons is

$$\phi(\tau,E,\mu) = \Phi(E)\, e^{\tau/\mu} - \int_0^{\tau} \frac{dt}{\mu}\, e^{(\tau-t)/\mu}$$
$$\left\{ b(E)\ \phi(b(E)*t, E+W, \mu) - r(E)*\phi(t,E,\mu) \right.$$
$$\left. + r(E) \int_{-1}^{+1} d\mu'\ p(E,\mu',\mu)*\phi(t,E,\mu') \right\} \qquad (12)$$

$-1 \leq \mu < 0$ and

$$\phi(\tau,E,\mu) = \int_{\tau}^{\infty} \frac{dt}{\mu}\, e^{(\tau-t)/\mu}$$
$$*\left\{ b(E)*\phi(b(E)*t,\ E+W, \mu) - r(E)*\phi(t,E,\mu) \right.$$
$$\left. + r(E) \int_{-1}^{1} d\mu'\ p(E,\mu',\mu)*\phi(t,E,\mu') \right\} \qquad (13)$$

for $0<\mu\leq 1$.

$$\phi(E) = \left(\frac{K_1^* Q_s}{2\pi\ E_o^3}\right) E \exp\ (-\ E/E_o) \qquad (14)$$

and K_1, Q_s, and E_o are constants with

$$b(E) = \frac{Q(E+W)}{Q(E)}\ ,\ r(E) = QE'(E)/Q(E)$$

Q(E) and QE'(E) are defined by logarithmic interpolation o bles of Q(E) versus E and QE'(E) versus E respectively.

$$p(E,\mu',\mu) = \frac{2\eta(E)*(1+\eta(E))*(1+2\eta(E)-\mu'\mu)}{\left[(1+2\eta(E)-\mu'\mu)^2 - (1-\mu^2)*(1-\mu'^2)\right]^{3/2}} \qquad (15)$$

where $\eta(E)$ is found by logarithmic interpolation of a table of $\eta(L)$ versus E values.

The integral equations were approximated for a set of N_E, E_i values E_{MIN}, $E_{MIN} + W$, $E_{MIN} + 2W, \ldots, E_{MAX}$, a set of N_τ, τ_j values $0, \tau_2, \tau_3, \ldots, \tau_{MAX}$ $(\tau_\ell < \tau_{\ell+1})$ and a set of N_μ, μ_k values $-1, \ldots, 0^-, 0^+, \ldots, 1$. $(\mu_\ell < \mu_{\ell+1})$.

The μ integrations $\left(\int_{-1}^{1} d\mu' \text{ etc.}\right)$ were rewritten as $\left(\int_{-1}^{0-} d\mu' \text{ etc.}\right) + \left(\int_{0+}^{1} d\mu' \text{ etc.}\right)$ because $\phi(\tau,E,\mu)$ may be discontinuous at $\phi(\tau,E,0)$. The following procedure describes the technique used to determine $\phi(\tau,E,0)$.

Rewriting (12) and (13), we have

$$\phi(\tau,E,\mu) = \phi(E)\, e^{\tau/\mu} - \int_0^{\tau} \frac{dt}{\mu}\, e^{(\tau-t)/\mu}\left\{F(t,E,\mu)\right\} \tag{16}$$

for $-1 \leq \mu \leq 0$ and

$$\phi(\tau,E,\mu) = \int_{\tau}^{\infty} \frac{dt}{\mu}\, e^{(\tau-t)/\mu}\left\{F(t,E,\mu)\right\} \tag{17}$$

where

$$F(t,E,\mu) = b(E)*\phi(b(E)*t,E+W,\mu) - (r(E)*\phi)(t,E,\mu) + r(E) \int_{-1}^{1} d\mu'\, p(E,\mu',\mu)*\phi(t,E,\mu') \ . \tag{18}$$

As $\mu \to 0^-$ in (16) and $\mu \to 0^+$ in (17), $F(t,E,\mu) \Rightarrow F(t,E,0^-)$ and $F(t,E,0^+)$ respectively.

Thus $\phi(\tau,E,0^-) = -F(\tau,E,0^-) \int_{\tau}^{\infty} \frac{dt}{0^-}\, e^{(\tau-t)/0^-}$ since

$e^{(\tau-t)/0^-} = 0$ for $t > 0^-$.

Hence,

$$\phi(\tau,E,0^-) = -F(\tau,E,0^-) \left[e^{(\tau-t)/0^-}\right]_{t}^{\infty} = F(\tau,E,0^-) \ . \tag{19}$$

Similarly

$$\phi(\tau,E,0^+) = +F(\tau,E,0^+) \int_0^{t} \frac{dt}{0^+}\, e^{(\tau-t)/0^+} = +F(\tau,E,0^+) \left[e^{(\tau-t)/0^+}\right]_{0}^{\tau}$$

$$= F(\tau,E,0^+) \ . \tag{20}$$

Now consider

$$G(\tau,E,\mu) = -r(E)*\phi(t,\mu,E) + r(E)* \int_{-1}^{1} d\mu'\, p(E,\mu',\mu)*\phi(t,E,\mu')$$

with the assumption that for values of μ' such that $\mu_k \leq \mu' \leq \mu_{k+1}$

$$Q(t,E,\mu') = \frac{(\mu_{k+1}-\mu')}{(\mu_{k+1}-\mu_k)}\ \phi(t,E,\mu_k) + \frac{(\mu'-\mu_k)}{(\mu_{k+1}-\mu_k)}\ \phi(t,E,\mu_{k+1})$$

where linear interpolation is used. Then

$$G(\tau,E,\mu) = -r(E)\ \phi(t,\mu,E) + r(E) \sum_{k=1}^{N_\mu - 1} \left(\int_{\mu_k}^{\mu_{k+1}} d\mu'\ p(E,\mu',\mu) * \phi(t,E,\mu') \right)$$

where

$$\int_{0^-}^{0^+} d\mu'\ p(E,\mu',\mu) * \phi(t,E,\mu') = 0 \tag{21}$$

$$\Rightarrow G(\tau,E,\mu) = -r(E)\ \phi(t,\mu,E) + r\ (E) \sum_{k=1}^{N_\mu - 1} \left(\int_{\mu_k}^{\mu_{k+1}} d\mu'\ p(E,\mu'\mu) \right.$$

$$\left(\frac{\mu_{k+1}}{\mu_{k+1} - \mu_k}\ \phi(t,E,\mu_k) - \frac{\mu'}{\mu_{k+1} - \mu_k}\ \phi(t,E,\mu_k) - \frac{\mu_k}{\mu_{k+1} - \mu_k}\ \phi(t,E,\mu_{k+1}) \right.$$

$$\left. \left. + \frac{\mu'}{\mu_{k+1} - \mu_k}\ \phi(t,E,\mu_{k+1}) \right) \right) \tag{22}$$

Now consider

$$p(E,\mu',\mu) = \frac{2\eta(E) * (1+\eta(E)) * (1+2\eta(E) - \mu'\mu)}{\left[(1+2\eta(E)-\mu\mu')^2 - (1-\mu'^2) * (1-\mu^2) \right]^{3/2}}, \quad \mu \neq 1 \tag{23}$$

$$= \frac{2\eta(E)*(1+\eta(E))*(1+2\eta(E)) - 2\eta(E)*(1+\eta(E)) * \mu\mu'}{\left[4\eta(E) + 4\eta^2(E) + \mu^2 - (2\mu+4\eta(E)*\mu)\ \mu' + \mu'^2 \right]^{3/2}}$$

$$\equiv \frac{U + V\mu'}{\left[a+b\mu'+\mu'^2 \right]^{3/2}} . \tag{24}$$

In equation (24),

$$\left.\begin{aligned} U &= 2\eta(E)*(1+\eta(E))*(1+2\eta(E)),\ V = -2\eta(E)*(1+\eta(E))*\mu \\ a &= 4\eta(E) + 4\eta^2(E) + \mu^2 \qquad ,\ b = -(2\mu+4\eta(E)*\mu) \end{aligned}\right\} \tag{25}$$

Therefore, if $\mu \neq \pm 1$

$$\int_{\mu_k}^{\mu_{k+1}} d\mu'\ p(E,\mu'\mu) \left(\frac{\mu_{k+1}}{\mu_{k+1}-\mu_k}\ \phi(t,E,\mu_k) - \frac{\mu'}{\mu_{k+1}-\mu_k}\ \phi(t,E,\mu_k)\right.$$

$$\left. - \frac{\mu_k}{\mu_{k+1}\ \mu_k}\ \phi(t,E,\mu_{k+1}) + \frac{\mu'}{(\mu_{k+1}-\mu_k)}\ \phi(t,E,\mu_{k+1})\right)$$

$$= \int_{\mu_k}^{\mu_{k+1}} d\mu' \left[\left(\frac{A_{k,k} + B_{k,k}\ \mu' + C_{k,k}\mu'^2}{R^{3/2}(\mu')}\right)\ \phi(t,E,\mu_k)\right.$$

$$\left. + \left(\frac{A_{k,k+1} + B_{k,k+1}\ \mu' + C_{k,k+1}\ \mu'^2}{R^{3/2}(\mu')}\right)\ \phi(t,E,\mu_{k+1})\right] \tag{26}$$

where $R(\mu') = a + b\mu' + \mu'^2$

$$A_{k,k} = U\ \frac{\mu_{k+1}}{(\mu_{k+1}-\mu_k)}\ ,\ B_{k,k} = (V\ \mu_{k+1}-U)/(\mu_{k+1}-\mu_k)\ ,$$

$$C_{k,k} = -V/(\mu_{k+1}-\mu_k),\ A_{k,k+1} = -U\ \frac{\mu_k}{(\mu_{k+1}-\mu_k)}\ ,\ \text{and}$$

$$B_{k,k+1} = (U-V\mu_k)/(\mu_{k+1}-\mu_k),\ C_{k,k+1} = \frac{V}{(\mu_{k+1}-\mu_k)}\ . \tag{27}$$

Letting

$$\Delta = 4a-b^2 = 16\eta(E)*(1+\eta(E))*(1-\eta^2)\ ,\ \Delta \neq 0$$

$$\left.\begin{aligned}
&\int \frac{d\mu'}{R^{3/2}(\mu')} = \frac{2*(2\mu'+b)}{\Delta*R^{1/2}(\mu')} \\
&\int \frac{\mu' d\mu'}{R^{3/2}(\mu')} = -\frac{2*(2a+b\mu')}{\Delta*R^{1/2}(\mu')} \\
&\int \frac{\mu'^2 d\mu'}{R^{3/2}(\mu')} = -\frac{(\Delta-b^2)\,\mu'-2ab}{\Delta*R^{1/2}(\mu')} \\
&\quad + \ln(2R^{1/2}(\mu') + 2\mu' + b).
\end{aligned}\right\} \tag{28}$$

and

Then

$$\begin{aligned}
\int_{\mu_k}^{\mu_{k+1}} d\mu' \Bigg[&\left(\frac{A_{k,k} + B_{k,k}\mu' + C_{k,k}\mu'^2}{R^{3/2}(\mu')} \right) \phi(t,E,\mu_k) \\
&+ \left(\frac{A_{k,k+1} + B_{k,k+1}\mu' + C_{k,k+1}\mu'^2}{R^{3/2}(\mu')} \right) \phi(t,E,\mu_{k+1}) \Bigg] \\
&= D_{k,k}\ \phi(t,E,\mu_k) + D_{k,k+1}\ \phi(t,E,\mu_{k+1})
\end{aligned} \tag{29}$$

where $\phi(t,E,\mu_k)$ and $\phi(t,E,\mu_{k+1})$ are constants to be calculated.

From equation (29),

$$\begin{aligned}
D_{k,L} = {} & A_{k,L} \left[\frac{2(2\mu_{k+1}+b)}{\Delta*R^{1/2}(\mu_{K+1})} - \frac{2(2\mu_K+b)}{\Delta*R^{1/2}(\mu_k)} \right] \\
& + B_{k,L} \left[-\frac{2(2a+b\mu_{K+1})}{\Delta*R^{1/2}(\mu_{K+1})} + \frac{2(2a+b\mu_K)}{\Delta*R^{1/2}(\mu_K)} \right] \\
& + C_{k,L} \left[-\frac{(\Delta-b^2)\mu_{K+1} - 2ab}{\Delta*R^{1/2}(\mu_{K+1})} + \frac{(\Delta-b^2)\mu_K - 2ab}{\Delta*R^{1/2}(\mu_K)} \right. \\
& \left. + LN\left(\frac{2R^{1/2}(\mu_{K+1}) + 2\mu_{K+1} + b}{2R^{1/2}(\mu_K) + 2\mu_K + b} \right) \right]
\end{aligned} \tag{30}$$

for L=k and L+1.

Now μ_m will be evaluated at one of the set of μ_K values (say μ_m) and

$$-r(E)\ \phi(t,E,\mu_m) + r(E) \int_{-1}^{1} d\mu'\ p(E,\mu',\mu_m) = \sum_{k=1}^{N_\mu} J_K(\mu_m)\ \phi(t,E,\mu_K) \qquad (31)$$

where

$$J_K = r(E)\ (D_{k,k} + D_{k-1,k} - \delta_{m,k}) \qquad (32)$$

with $D_{0,1} = D_{N_\mu,N_\mu} = 0$.

If $\mu_m = \mu = \pm 1$, then

$$p(E,\mu',\mu_m) = \frac{2\eta(E)(1+\eta(E))}{(1+2\eta(E)-\mu_m\mu')^2} \qquad (33)$$

or

$$p(E,\mu',\mu_m) = \frac{C}{(d+e\mu')^2} \qquad (34)$$

where $C=2\eta(E)(1+\eta(E))$; $d=1+2\eta(E)$ and $e=-\mu_m$. Equation (26) for $\mu = \mu_m = \pm 1$ now becomes

$$\int_{\mu_K}^{\mu_{K+1}} d\mu'\ p(E,\mu',\mu) \left(\frac{\mu_{K+1}}{(\mu_{K+1}-\mu_K)}\ \phi(t,E,\mu_K) - \frac{\mu'}{(\mu_{K+1}-\mu_k)}\ \phi(t,E,\mu_K) \right.$$

$$\left. - \frac{\mu_K}{(\mu_{K+1}-\mu_K)}\ \phi(t,E,\mu_{K+1}) + \frac{\mu'}{(\mu_{K+1}-\mu_K)}\ \phi(t,E,\mu_{K+1}) \right)$$

$$= \int_{\mu_K}^{\mu_{K+1}} d\mu' \left(\frac{E_{k,k}}{(d+e\mu')^2}\ \phi(t,E,\mu_K) + \frac{E_{k,k}\ \mu'}{(d+e\mu')^2}\ \phi(t,E,\mu_K) \right)$$

$$+ \left(\frac{E_{k,k+1}}{(d+e\mu')^2}\ \phi(t,E,\mu_{K+1}) + \frac{E_{k,k+1}\ \mu'}{(d+e\mu')^2}\ \phi(t,E,\mu_{K+1}) \right) \qquad (35)$$

where

$$E_{k,k} = \frac{C\ \mu_{K+1}}{(\mu_{K+1}-\mu_K)} \quad , \quad E_{K,K} = \frac{-C}{(\mu_{K+1}-\mu_K)} \quad ,$$

$$E_{k,k+1} = -\frac{C\mu_k}{(\mu_{K+1}-\mu_K)} \quad E_{K,K+1} = \frac{C}{\mu_{K+1}-\mu_K}$$

However,

$$\left.\begin{aligned} \int \frac{d\mu'}{(d+e*\mu')^2} &= -\frac{1}{e(d+e*\mu')} \\ \text{and} \\ \int \frac{d\mu'\ \mu'}{(d+e*\mu')^2} &= -\frac{-\mu'}{e(d+e*\mu')} + \frac{1}{e^2}\ \ln\ (d+e*\mu') \end{aligned}\right\} \quad (36)$$

Therefore for $\mu_m = \mu = \pm 1$,

$$\int_{\mu_k}^{\mu_{k+1}} d\mu' \left[\left(\frac{E_{K,K} + \mu' F_{K,K}}{(d+e*\mu')^2}\right) \phi(t,E,\mu_K) + \left(\frac{E_{K,K+1} + \mu' F_{K,K+1}}{(d+e*\mu')^2}\right) \phi(t,E,\mu_{K+1})\right]$$

$$= D_{k,k}\ \phi(t,E,\mu_K) + D_{k,k+1}\ \phi(t,E,\mu_{K+1}) \ . \quad (37)$$

When $\mu_m = \mu = \pm 1$,

$$D_{k,L} = \frac{1}{e}\left(\frac{1}{(d+e*\mu_K)} - \frac{1}{(d+e*\mu_{K+1})}\right)\ E_{K,L} + \left(\frac{1}{e}\left(\frac{\mu_K}{(d+e*\mu_K)} - \frac{\mu_{K+1}}{(d+e*\mu_{K+1})}\right) + \frac{1}{e^2}\ \ln\left(\frac{d+e*\mu_{K+1}}{d+e*\mu_K}\right)\right) F_{K,L} \ . \quad (38)$$

For L=k and $\ell = k+1$ in the above expressions, (31) then holds for $\mu_m = \mu = \pm 1$.

Now consider the term

$$T = b(E)*\phi(b(E)t, E+W, \mu_m) \quad (39)$$

We wish to evaluate T for $E=E_i$, $i=1,\ldots,N_E$. If $E_i \cdot E_{MAX} = E_{N_E}$, T can be found by linearly interpolating on t to get

$$T = b(E)\left(\frac{(\tau_{j+1} - b(E)t)}{(\tau_{j+1} - \tau_j)}\ \phi(\tau_j, E+W, \mu_m) + \frac{(b(E)t - \tau_j)}{(\tau_{j+1} - \tau_j)}\ \phi(\tau_{j+1}, E+W, \mu_m)\right) \quad (40)$$

where $\tau_j - b(E)t \leq \tau_{j+1}$ and $E<E_{MAX}$. Then

$$T = H^{E}_{j,j} * \phi(\tau_j, E+W, \mu_m) + I^{E}_{j,j} * t * \phi(\tau_j, E+W, \mu_m)$$

$$+ H^{E}_{j,j+1} * \phi(\tau_{j+1}, E+W, \mu_m) + I^{E}_{j,j+1} * t * \phi(\tau_{j+1}, E+W, \mu_m) \tag{41}$$

where

$$H^{E}_{j,j} = -\frac{b(E)\,\tau_{j+1}}{(\tau_{j+1}-\tau_j)} \quad , \quad I^{E}_{j,j} = -\frac{b^2(E)}{\tau_{j+1}-\tau_j}$$

$$H^{E}_{j,j+1} = -\frac{b(E)\,\tau_j}{(\tau_{j+1}-\tau_j)} \quad , \quad I^{E}_{j,j+1} = \frac{b^2(E)}{\tau_{j+1}-\tau_j} \quad .$$

If $E_i = E_{MAX} = E_{N_E}$ it is assumed that as $E \to \infty$

$$\phi(\tau_j, E+W, \mu_m) = \phi(\tau_j, E, \mu_m)\,\frac{E+W}{E}\,e^{-\alpha(\tau_j, \mu_m)\,W} \tag{42}$$

where $\alpha(\tau_j, \mu_m)$ is a set of input data values. For the case $E=E_{MAX}$ we will then have

$$T = H^{E_{MAX}}_{j,j} * \phi(\tau_j, E_{MAX}, \mu_m) + I^{E_{MAX}}_{j,j} * t * \phi(\tau_j, E_{MAX}, \mu_m)$$

$$+ H^{E_{MAX}}_{j,j+1} * \phi(\tau_{j+1}, E_{MAX}, \mu_m) + I^{E_{MAX}}_{j,j+1} * t\phi(\tau_{j+1}, E_{MAX}, \mu_m)$$

where

$$H^{E_{MAX}}_{j,L} = K * \frac{b(E_{MAX})}{b(E)} H^{E}_{j,L} \text{ and } I^{E_{MAX}}_{j,L} = K * \left(\frac{b(E_{MAX})}{b(E)}\right)^2 I^{E}_{j,L} \quad . \tag{43}$$

In the above equation, $E = E_{MAX}$

for $L = j$ and $L = j+1$, and $K = \frac{E_{MAX}+W}{E_{MAX}}\,e^{-\alpha(\tau_j, \mu_m)\,W}$.

Using the above results we now wish to calculate

$$S_1(\tau,E,\mu) = \int_0^{\tau} \frac{dt}{\mu}\, e^{(\tau-t)/\mu} \left\{F(t,E,\mu)\right\}$$

or

$$S_2(\tau,E,\mu) = -\int_{\tau}^{\infty} \frac{dt}{\mu}\, e^{(\tau-t)/\mu} \left\{F(t,E,\mu)\right\} . \qquad (44)$$

From equations (19) and (20)

$$S_1 = F(\tau,E,o) = S_2 \qquad (45)$$

When $\mu \neq o$, $\mu = \mu_m$,

$$EW = E+W*(1-\delta_{E,E_{MAX}}) \qquad (46)$$

b(E) is assumed <1, $\tau_\ell < \tau_{N\tau}$, and $\tau_\ell \leq t \leq \tau_{\ell+1}$. These assumptions can be satisfied so long as $\tau \leq \tau_{N\tau}$.

We can then express

$$F(t,E,\mu_m) = H^E_{j,j} * \phi(\tau_j, EW, \mu_m) + I^E_{j,j} * t * \phi(\tau_j, EW, \mu_m)$$

$$- H^E_{j,j+1} * \phi(\tau_{j+1}, EW, \mu_m) + I_{j,j+1} * t * \phi(\tau_{j+1}, EW, \mu_m)$$

$$+ \sum_{k=1}^{N_\mu} J_K(\mu_m) * (K_{\ell,\ell}\phi(\tau_\ell, E, \mu_k) + L_{\ell,\ell} * t * \phi(\tau_\ell, E, \mu_k)$$

$$+ K_{\ell,\ell+1} * \phi(\tau_{\ell+1}, E, \mu_k) + L_{\ell,\ell+1} * t * \phi(\tau_{\ell+1}, E, \mu_k)) \qquad (47)$$

where we have used equations (31), (41) and (43) while assuming linear interpolation between τ_ℓ and $\tau_{\ell+1}$. Now

$$K_{\ell,\ell} = \frac{\tau_{\ell+1}}{(\tau_{\ell+1}-\tau_\ell)} \quad , \quad L_{\ell,\ell} = -\frac{1}{(\tau_{\ell+1}-\tau_\ell)}$$

$$K_{\ell,\ell+1} = -\frac{\tau_\ell}{(\tau_{\ell+1}-\tau_\ell)} \quad , \quad L_{\ell,\ell+1} = \frac{1}{(\tau_{\ell+1}-\tau_\ell)} \qquad (48)$$

In order to evaluate S_1 in (44), we note that

$$S_1(\tau_j,E,\mu) = e^{-\frac{(\tau_j-\tau_{j-1})}{\mu}} S_1(\tau_{j-1},E,\mu) + \int_{\tau_{j-1}}^{\tau_j} \frac{dt}{\mu}\ e^{(\tau-t)/\mu}\{F(t,E,\mu)\}. \qquad (49)$$

Using this fact we first evaluate $S_1(\tau_2,E,\mu)$ ($S_1(\tau_1,E,\mu) = 0$ since $\tau_1=0$). We then use this result to evaluate $S_1(\tau_3,E,\mu)$ and continue this procedure recursively until we evaluate $S_1(\tau_{N_\tau},E,\mu)$.

Similarly in order to evaluate S_2 in (44), we note that

$$S_2(\tau_j,E,\mu) = e^{(\tau_j-\tau_{j+1})/\mu} S_2(\tau_{j+1},E,\mu) + \int_{\tau_j}^{\tau_{j+1}} \frac{dt}{\mu}\ e^{(\tau-t)/\mu}\{F(t,E,\mu)\}. \qquad (50A)$$

Thus, we first evaluate $S_2(\tau_{N_\tau},E,\mu)$. We then use this result to evaluate $S_2(\tau_{(N_\tau-1)},E,\mu)$ and continue this procedure recursively until we evaluate $S_2(\tau_1=0,E,\mu)$.

Enough information has been provided to calculate the S_1 and S_2 values, so long as $S_2(\tau_{N_1},E,\mu)$ can be evaluated. In order to evaluate $S_2(\tau_{N_\tau},E,\mu)$, the following model is used:

$$\text{Let } \mu_0 = \mu_1 \text{ and } \mu(N_{\mu+1}) = \mu_{N_M}, \qquad (50B)$$

$$\alpha(E,\mu) = \alpha(E,\mu_j)$$

for

$$\frac{(\mu_{j-1}+\mu_j)}{2} < \mu \le \frac{(\mu_j+\mu_{j+1})}{2}.$$

The values of $\alpha(E,\mu_j)$ are found by interpolating a table of $\alpha(E,\mu)$ versus E and μ, which is provided as input data. The values of $\phi(\tau,E,\mu)$ with $\tau>\tau_{N_\tau}$ are then assumed to be

$$\phi(\tau,E,\mu) = \phi(\tau_{N_\tau},E,\mu)\, e^{-(\tau-\tau_{N_\tau})\,\alpha(E,\mu)}. \qquad (51)$$

With this model we calculate $S_2(\tau_{N_\tau}, E, \mu)$ as

$$S_2(\tau_{N_\tau}, E, \mu_m) \quad -\int_{\tau_{N_\tau}}^{\infty} \frac{dt}{\mu_m} e^{(\tau_{N_\tau}-t)/\mu_m} \left\{F(t,E,\mu)\right\}$$

$$= -\int_{b\tau_{N_\tau}}^{\tau_{N_\tau}} \frac{dt}{\mu_m} e^{(\tau_N-t)/\mu_m} \left\{H^E_{j,j}\ \phi(\tau_j, EW, \mu_m) + I^E_{j,j} * t * \phi(\tau_j, EW, \mu_m)\right.$$

$$\left. + H^E_{j,j+1} * \phi(\tau_{j+1}, EW, \mu_m) + I_{j,j+1} * t * \phi(\tau_{j+1}, EW, \mu_m)\right.$$

$$-\int_{\tau_{N_\tau}}^{\infty} \frac{ds}{\mu_m} e^{\frac{(\tau_{N_\tau} - \frac{s}{b(E)})}{\mu_m}} \phi(\tau_{N_\tau}, EN, \mu_m)\ e^{-(s-\tau_{N_\tau})\ \alpha(E,\mu_m)}$$

$$-\int_{\tau_N}^{\infty} dt \left\{G(\tau, E, \mu_m)\ e^{(\tau_N - t)/\mu_m} \right\} \qquad (52)$$

where the integration from $b\tau_{N_\tau}$ to τ_{N_τ} is described in (53) and (54). The integral over ds is found by the substitution $s=b(E)t$ and is described in (55) and (56). The integral of $G(\tau,E,\mu_m)$ (see equation (21)) appears in (64).

Thus we have

$$TR = -\int_a^b \frac{dt}{\mu_m}\ e^{\frac{(\tau-t)}{\mu_m}} \left\{H^E_{j,j}\ \phi(\tau_j, EW, \mu_m) + I^E_{j,j}\ t\phi(\tau_j, EW, \mu_m)\right.$$

$$\left. + H^E_{j,j+1}\ \phi(\tau_{j+1}, EW, \mu_m) + I_{j,j+1} * t * \phi(\tau_{j+1}, EW, \mu_m)\right\}$$

$$= -\sum_{j=1}^{(N_\tau-1)} \int_{as(j)}^{bs(t)} \frac{dt}{\mu_m} e^{(\tau-t)/\mu_m} \left\{H^E_{j,j}\ \phi(\tau_j, EW, \mu_m) + I^E_{j,j} * t * \phi(\tau_j, EW, \mu_m)\right.$$

$$\left. + H^E_{j,j+1} * \phi(\tau_{j+1}, EW, \mu_m) + I_{j,j+1} * t * \phi(\tau_{j+1}, EW, \mu_m)\right\} \qquad (53)$$

where

$a = b = \tau_{N_\tau}$, $as(j) = \text{maximum}(a, \tau_j)$

$bs(j) = \text{minimum}(b, \tau_{j+1})$, and $as(j) < bs(j)$.

$$TR = + \sum_{j=1}^{(N_\tau - 1)} \left\{ \left(e^{(\tau - bs(j))/\mu_m} - e^{(\tau - as(j))/\mu_m} \right) \left(H^E_{j,j} * \phi(\tau_j, EW, \mu_m) \right. \right.$$

Integrating we get

$$+ H^E_{j,j+1} \phi(\tau_{j+1}, EW, \mu_m)) + (bs(j) + \mu_m) \, e^{(\tau - bs(j))/\mu_m}$$

$$- \left(as(j) + \mu_m \right) e^{(\tau - as(j))/\mu_m} \Big) \left(I^E_{j,j} * \phi(\tau_0, EW, \mu_m) \right.$$

$$\left. \left. + I^E_{j,j+1} * \phi(\tau_{j+1}, EW, \mu_m) \right) \right\} \tag{54}$$

We also have

$$TR1 = - \int_{\tau_{N_\tau}}^{\infty} \frac{ds}{\mu_m} \; e^{\left(\tau_{N_\tau} \left(\frac{1}{\mu_m} + \alpha(E, \mu_m) \right) - s \left(1/b(E)\mu_m + \alpha(EW, \mu_m) \right) \right)} \phi(\tau_{N_\tau}, EW, \mu_m) \tag{55}$$

Integrating we get

$$TR1 = - \frac{b(E)\mu_m}{(1 + b(E)\,\mu_m \alpha(EW, \mu_m))} \left(e^{\tau_{N_\tau} (1/\mu_m - 1/b(E)\mu_m)} \right) . \tag{56}$$

We also have

$$TR2 = - \int_{\tau_{N_\tau}}^{\infty} dt \left\{ G(\tau, E, \mu_m) \right\} . \tag{57}$$

Using the model for $\alpha(E, \mu_m)$ in (50B) and the expression for $G(\tau, E, \mu)$ in (22).

$$TR2 = -\int_{\tau_{N_\tau}}^{\infty} \frac{1}{\mu_m} e^{(\tau_{N_\tau}-t)/\mu_m} (-r(E)*\phi(\tau_N,\mu,E)\, e^{-(\tau_{N_\tau}-t)\alpha(E,\mu_m)}$$

$$+ r(E) \sum_{k=1}^{N_\mu-1} \left(\left(\int_{\mu_k}^{\frac{\mu_k+\mu_{k+1}}{2}} d\mu'\, p(E,\mu',\mu)\, \frac{\mu_{k+1}}{\mu_{k+1}-\mu_k}\, \phi(\tau_{N_\tau},E,\mu_k) \right.\right.$$

$$e^{-(\tau_{N_\tau}-t)*\alpha(E,\mu_k)}$$

$$- \frac{\mu'}{\mu_{k+1}-\mu_k}\, \phi(\tau_{N_\tau},E,\mu_k)\, e^{-(\tau_{N_\tau}-t)\alpha(E,\mu_k)} - \frac{\mu_k}{(\mu_{k+1}-\mu_k)}\, \phi(\tau_{N_\tau},E,\mu_{k+1})$$

$$e^{-(\tau_N-t)*\alpha(E,\mu_k)}$$

$$\left. + \frac{\mu'}{\mu_{k+1}-\mu_k}\, \phi(\tau_{N_\tau},E,\mu_{k+1})\, e^{-(\tau_{N_\tau}-t)\alpha(E,\mu_k)} \right) + \left(\int_{\mu_k+\mu_{k+1}/2}^{\mu_{k+1}} p(E,\mu',\mu) \right.$$

$$\left(\frac{\mu_{k+1}}{(\mu_{k+1}-\mu_k)}\, \phi(\tau_{N_\tau},E,\mu_k)\, e^{-(\tau_{N_\tau}-t)*\alpha(E,\mu_{k+1})} - \frac{\mu'}{(\mu_{k+1}-\mu_k)}\, \phi(\tau_{N_\tau},E,\mu_k) \right.$$

$$e^{-(\tau_{N_\tau}-t)*\alpha(E,\mu_{k+1})}$$

$$\left. - \frac{\mu_k}{(\mu_{k+1}-\mu_k)}\, \phi(\tau_{N_\tau},E,\mu_{k+1})\, e^{-(\tau_{N_\tau}-t^*(E,\mu_{k+1})} + \frac{\mu'}{(\mu_{k+1}-\mu_k)}\, \phi(\tau_{N_\tau},E,\mu_{k+1}) \right)$$

$$e^{-(\tau_{N_\tau}-t)*\alpha(E,\mu_{k+1})} \qquad (58)$$

Using results of analyses described in (29) through (32) and (58), we have

$$TR2 = -\int_{\tau_{N_\tau}}^{\infty} \frac{1}{\mu_m} e^{(\tau_{N_\tau} - t)/\mu} \sum_{k=1}^{N_\mu} \left(J_K^{(-)}(\mu_m) * \phi(\tau_{N_\tau}, E, \mu_k)\, e^{-(t-\tau_{N_\tau})\alpha(E,\mu_{k-1})} \right.$$

$$+ J_K^{(10)}(\mu_m) * \phi(\tau_{N_\tau}, E, \mu_k)\, e^{-(t-\tau_{N_\tau})\alpha(E,\mu_k)} + J_K^{(+)}(\mu_m) * \phi(\tau_{N_\tau}, E, \mu_k)$$

$$\left. e^{-(t-\tau_{N_\tau})*\alpha(E,\mu_{k+1})} \right) \tag{59}$$

where

$$\left.\begin{aligned} J_K^{(-)} &= r(E)\, D_{k-1,k}^{(-)} + r(E)\,(D_{k,k}^{(0)} + D_{k-1,k}^{(0)} - \delta_{mk}) \\ &\qquad\qquad \text{and} \\ J_K^{(+)} &= r(E)\, D_{k,k}^{(+)} \end{aligned}\right\} \tag{60}$$

with

$$D_{0,1}^{(-)} = D_{0,1}^{(0)} = 0 \quad . \tag{61}$$

Now let

$$\mu_K^{MID} = \frac{(\mu_K + \mu_{K+1})}{2} \quad . \tag{62}$$

If $|\mu| \neq 1$ in (30), then

$$D_{k,k+1}^{(-)} = A_{k,k+1} \left[\frac{2(2\mu_{k+1}+b)}{\Delta^* R^{1/2}(\mu_{K+1})} - \frac{2(2\mu_K^{MID}+b)}{\Delta^* R^{1/2}(\mu_K^{MID})} \right]$$

$$+ B_{k,k+1} \left[\frac{2(2a+b\mu_{K+1})}{\Delta^* R^{1/2}(\mu_{K+1})} + \frac{2(2a+b\mu_K^{MID})}{\Delta^* R^{1/2}(\mu_K^{MID})} \right]$$

$$+ C_{k,k+1} \left[\frac{(\Lambda - b^2)\,\mu_{K+1} - 2ab}{\Delta^* R^{1/2}(\mu_{K+1})} + \frac{2(2a+b\mu_K^{MID})}{\Delta^* R^{1/2}(\mu_K)} \right.$$

$$\left. + LN\left(\frac{2R^{1/2}(\mu_{K+1}) + 2\mu_{K+1} + b}{2R^{1/2}(\mu_K^{MID}) + 2\mu_K^{MID} + b} \right) \right] \tag{63A}$$

$$D^{(0)}_{k,L} = A_{K,L}\left[\frac{2(2\mu_K^{MID}+b)}{\Delta^* R^{1/2}(\mu_K^{MID})} - \frac{2(2\mu_K+b)}{\Delta^* R^{1/2}(\mu_K)}\right]$$

$$+ B_{K,L}\left[\frac{-2(2a+b\mu_K^{MID})}{\Delta^* R^{1/2}(\mu_K^{MID})} + \frac{2(2a+b\mu_K)}{\Delta^* R^{1/2}(\mu_K)}\right]$$

$$+ C_{k,L}\left[\frac{-(\Delta-b^2)\ \mu_K^{MID}-2ab}{\Delta^* R^{1/2}(\mu_K^{MID})} + \frac{(\Delta-b^2)\ \mu_K-2ab}{\Delta^* R^{1/2}(\mu_K)}\right.$$

$$\left. + LN\left(\frac{2R^{1/2}(\mu_K^{MID}) + 2\mu_K^{MID} + b}{2R^{1/2}(\mu_K) + 2\mu_K + b}\right)\right] \qquad (63B)$$

for L=k and L=k+1, and

$$D^{(+)}_{k,k} = A_{k,k}\left[\frac{2(2\mu_{K+1}+b)}{\Delta^* R^{1/2}(\mu_K^{MID})} - \frac{2(2\mu_k^{MID}+b)}{\Delta^* R^{1/2}(\mu_k^{MID})}\right]$$

$$+ B_{K,K}\left[\frac{-2(2a+b\mu_{K+1})}{\Delta^* R^{1/2}(\mu_{K+1})} + \frac{2(2a+b\mu_K^{MID})}{\Delta^* R^{1/2}(\mu_K^{MID})}\right]$$

$$+ C_{K,K}\left[\frac{-(\Delta-b^2)\ \mu_{K+1} - 2ab}{\Delta^* R^{1/2}(\mu_{K+1})} + \frac{(\Delta-b^2)\ \mu_K^{MID} - 2ab}{\Delta^* R^{1/2}(\mu_K^{MID})}\right.$$

$$\left. + LN\left(\frac{2R^{1/2}(\mu_{K+1}) + 2\mu_{K+1} + b}{2R^{1/2}(\mu_K^{MID}) + 2\mu_K^{MID} + b}\right)\right] . \qquad (63C)$$

From equation (38), if $|\omega| = 1$

$$D^{(-)}_{k,k+1} = \frac{1}{e}\left(\frac{1}{(d+e^*\mu_K^{MID})} - \frac{1}{(d+e^*\mu_{K+1})}\right)E_{k,k+1} + \frac{1}{e}\left(\left(\frac{\mu_K^{MID}}{(d+e^*\mu_K^{MID})} - \frac{\mu_{K+1}}{(d+e^*\mu_{K+1})}\right)\right.$$

$$\left. + \frac{1}{e^2}\ \ln\left(\frac{d+e^*\mu_{K+1}}{d+e^*\mu_K^{MID}}\right)\right)\ F_{k,k+1} \qquad (63D)$$

$$D_{k,L}^{(0)} = \frac{1}{e}\left(\frac{1}{(d+e^{*}\mu_K)} - \frac{1}{(d+e^{*}\mu_K^{MID})}\right)E_{k,L} + \left(\frac{1}{e}\left(\frac{K}{(d+e^{*}\mu_K)} - \frac{\mu_K^{MID}}{(d+e^{*}\mu_K^{MID})}\right)\right.$$

$$\left. + \frac{1}{e^2}\ln\left(\frac{d+e^{*}\mu_K^{MID}}{d+e^{*}\mu_K}\right)\right)E_{k,L} \qquad (63E)$$

for L=k and L k+1, and

$$D_{k,k}^{(+)} = \frac{1}{e}\left(\frac{1}{(d+e^{*}\mu_K^{MID})} - \frac{1}{(d+e^{*}\mu_{K+1})}\right)E_{k,k} + \frac{1}{e}\left(\left(\frac{\mu_K^{MID}}{(d+e^{*}\mu_K^{MID})} - \frac{K+1}{(d+e^{*}\mu_{K+1})}\right)\right.$$

$$\left. + \frac{1}{e^2}\ln\left(\frac{d+e^{*}\mu_{K+1}}{d+e^{*}\mu_K^{MID}}\right)\right)E_{k,k+1} \qquad (63F)$$

Noting that $J_K^{(-)}$, $J_K^{(0)}$ and $J_K^{(+)}$ of (59) are not functions of $\tau(t)$, we integrate (59) to get

$$TR2 = -\sum_{k=1}^{N_\mu}\frac{J_K^{(-)}*\phi(\tau_{N_\tau},E,\mu_K)}{\mu_m\left(\frac{1}{\mu_m}+\alpha(E,\mu_{k-1})\right)}$$

$$-\sum_{k=1}^{N_\mu}\frac{J_K^{(0)}*\phi(\tau_{N_\tau},E,\mu_K)}{\mu_m\left(\frac{1}{\mu_m}+\alpha(E,\mu_K)\right)}$$

$$-\sum_{k=1}^{N_\mu}\frac{J_K^{(+)}*\phi(\tau_{N_\tau},E,\mu_K)}{\mu_m\left(\frac{1}{\mu_m}+\alpha(E,\mu_{K+1})\right)} \qquad (64)$$

Using the preceding approximations for the behavior of $\phi(\tau,E,\mu)$ and the developed analyses, we can write (12) as

$$\phi(\tau_j,E_{MAX},\mu_k) = \phi(E_{MAX})\,e^{-\tau_j/\mu_k} + \sum_{L=1}^{N_\tau}\sum_{M=1}^{N_\mu}\left(O_{L,M}(\tau_j,E_{MAX},\mu_K)*\right.$$

$$\left.\phi(\tau_\ell,E_{MAX},\mu_M)\right) \qquad (65)$$

where $O_{L,M}(\tau_j, E_{MAX}, \mu_K)$ are constants, $\phi(E_{MAX})\, e^{\tau_j/0^-} = 0$ if $\tau_j \neq 0$, and $\phi(E_{MAX})\, e^{\tau_j/0^-} = \phi(E_{MAX})$ is $\tau_j = 0$. Now let

$$S_{L,M}(\tau_j, E_{MAX}, \mu_K) = \delta_{j,L}\,\delta_{k,M} - O_{L,M}(\tau_j, E_{MAX}, \mu_K) \tag{66}$$

($S_{L,M}(\tau_j, E_{MAX}, \mu_K)$ are constants)

Then (65) can be written as

$$\sum_{L=1}^{N_\tau} \sum_{M=1}^{N_\mu} S_{L,M}(\tau_j, E_{MAX}, \mu_K) * \phi(\tau_\ell, E_{MAX}, \mu_M) = \phi(E_{MAX})\, e^{\tau_j/\mu_k} . \tag{67}$$

Similarly (13) becomes

$$\sum_{L=1}^{N_\tau} \sum_{M=1}^{N_\mu} S_{L,M}(\tau_j, E_{MAX}, \mu_K) * \phi(\tau_\ell, E_{MAX}, \mu_M) = 0 \tag{68}$$

$$\text{for } \mu_K \geq 0^+ .$$

Equations (67) and (68) describe $N_\tau * N_\mu$ linear equations in $N_\tau * N_\mu$ unknowns ($\phi(\tau_j, E_{MAX}, \mu_k)$). This is solved using Gauss-Jordan reductions and the fact that if $\mu_K \leq 0^-$ (remembering $\tau_1 = 0$) when $\tau_j = \tau_1$, equation (67) becomes

$$\phi(\tau_1, E_{MAX}, \mu_k) = \phi(E_{MAX}) \quad . \tag{69}$$

Now assume we have found the solution for $\phi(\tau_j, E, \mu_k)$ when $E = E_{MAX}, E_{MAX}-W, E_{MAX}-2W \ldots, E_{i+1}$ and we want to find the solution for E_i. Using the derived numerical procedures, for $E_i < E_{MAX}$ equation (12) becomes

$$\phi(\tau_j, E_i, \mu_K) = \phi(E_i)\, e^{\tau_j/\tau_k} + \left(\sum_{L=1}^{N_\tau} \sum_{M=1}^{N_\mu} (O_{L,M}(\tau_j, E_i, \mu_K) * (\tau_\ell, E_i, \mu_M)) \right)$$

$$+ \left(\sum_{L=1}^{N_\tau} (W_L(\tau_j, E_i, \mu_K) * (\tau_\ell, E_{i+1}, \mu_K)) \right) \tag{70}$$

where $O_{L,M}(\tau_j, E_i, \mu_K)$ and $W_L(\tau_j, E_i, \mu_K)$ are constants. Then let

$$S_{L,M}(\tau_j, E_i, \mu_K) = \delta_{j,L}\,\delta_{k,M} - O_{L,M}(\tau_j, E_i, \mu_K) \tag{71}$$

Since we have already solved for $\phi(\tau_\ell, E_{i+1}, \mu_k)$ let

$$SUM(\tau_j, E_i, \mu_K) = \left(\sum_{L=1}^{N_\mu} (W_L(\tau_j, E_i, \mu_K) * \phi(\tau_\ell, E_{i+1}, \mu_k))\right) + \phi(E_i)\, e^{\tau_j/\mu_k} \tag{72}$$

for

$$\mu_K \leq 0^-$$

and be equal to

$$\left(\sum_{L=1}^{N_\mu} (W_L(\tau_j, E_i, \mu_K)\,\phi(\tau_\ell, E_{i+1}, \mu_k))\right) \tag{73}$$

for

$$\mu_K \geq 0^+ .$$

Then we can write (70) as

$$\sum_{L=1}^{N_\tau} \sum_{M=1}^{N_\mu} S_{L,M}(\tau_j, E_i, \mu_K) * \phi(\tau_\ell, E_i, \mu_M) = SUM(\tau_j, E_i, \mu_K) \tag{74}$$

for $\mu_K \leq 0^-$

and similarly (13) can be written as

$$\sum_{L=1}^{N_\tau} \sum_{M=1}^{N_\mu} S_{L,M}(\tau_j, E_i, \mu_K) * \phi(\tau_\ell, E_i, \mu_M) = SUM(\tau_j, E_i, \mu_K) \tag{75}$$

for $\mu_K \geq 0^+$.

Equations (74) and (75) describe $N_\tau * N_\mu$ linear equations in $N_\tau * N_\mu$ unknowns ($\phi(\tau_j, E_i, \mu_K)$). This system is solved using Gauss-Jordan reductions and the fact that when $\mu_K \leq 0^-$ and $\tau_j = \tau_1$, equation (74) becomes

$$\phi(\tau_1, E_i, \mu_K) = \phi(E_i) . \tag{76}$$

This completes the description of methods used to determine the electron flux $\phi(\tau, E, \mu)$.


DAT
ILM